Molecular Mechanisms of anti-carcinogenic Flavonoids

Honors Research Thesis

Presented in partial fulfillment of the requirements for graduation *with honors research distinction* in Molecular Genetics in the undergraduate colleges of The Ohio State University

by

Bledi Brahimaj

The Ohio State University
May 2011

Project Advisor: Dr. Andrea I. Doseff, Associate Professor,
Department of Molecular Genetics, Department of Internal Medicine

Index

Chapter 1: Introduction

1.1 Cancer

1.2 Flavonoids

1.3 Apigenin

1.4 Heterogeneous ribonucleoproteins

1.4a Heterogeneous ribonucleoprotein A2

Chapter 2: Materials and Methods

2.1 Plasmid Construction

2.2 Induction and Bacterial Cell Lysates

2.3 Protein Purification

2.4 Fluoresence Resonance Energy Transfer (FRET) Assay

2.5 Dissociation Constants

2.6 Tissue Culture & Treatment

2.7 RNA Isolation & Transcript Analysis

2.8 Western Blot

2.9 Bradford Assay

2.10 Migration Assay

Chapter 3: Results

3.1 Generation of a Flavonoid Nanosensor

3.2 Nanosensor Screening and Protein Expression

3.3 Multiple Flavonoids Interact with hnRNPA2

3.4 Apigenin and Invasive Lung Cancer Migration

Chapter 4: Discussion

Acknowledgements

References

1. Introduction:

1.1 Cancer

Cancer is the one of the most formidable burdens facing the United States, and other developed countries today. It is the leading cause of death worldwide that accounted for 7.6 million deaths in 2008, a number projected to increase in the future [1]. Current thought attributes carcinogenesis to a multi-step process of genetic and epigenetic abnormalities of normal cells [2]. Although progressive cancers have proven difficult to treat, cancer is a largely preventable disease, and through early detection and screening favorable prognosis ensues [2]. More than half of cancers can be prevented by avoiding exposure to carcinogens such as cigarette smoking, recurrent infections, and protection from excessive sun exposure and reductions in occupational and environmental toxins [3].

Of the vast type's cancers, lung cancer boasts both the highest rate of incidence and mortality [1]. Nearly 60% of individuals diagnosed with lung cancer die within a year of diagnosis. Adding to the lethality of the disease, there are few currently implemented screening methods for lung cancer and early detection markers are still being studied [4]. Also, many of the symptoms associated with lung cancer are common in other less serious conditions. There are two major types of lung cancer, small cell lung cancer (SCLC) and the more common non-small cell lung cancer (NSCLC), as characterized by histology. The faster growing and less common SCLC is further divided into three different types: small cell carcinoma, mixed small cell/large cell carcinoma and combined small cell carcinoma. SCLC is almost always caused by cigarette smoking. It metastasizes quickly form the bronchial tubes and is responsible for 15% of all lung cancer cases. NSCLC is also found in three different forms arising in different parts of the lungs. Adenocarcinomas are found in the outer area of the lung, squamous cell carcinomas are in the

center of the lung, near an air tube, and large cell carcinomas form throughout. Although more prevalent, NSCLC grows slower than its counterpart and is caused by smoking, pollution, arsenic and other environmental risk factors [5].

The molecular characteristics of NSCLC, include overexpression of nuclear factor-kappaB (NFκB). NFκB is a transcription factor that has been shown to play a role in cell proliferation and oncogenesis. Studies correlated NFκB expression with lung cancer differentiation in which higher expression of the transcription factor was inversely proportional to apoptotic rate [6]. The same study also observed a correlation of NFκB expression with cyclooxygenase-2, tumor suppressor p53 and the executioner of apoptosis caspase-3. Furthermore, the stress activated serine-threonine casein kinase 2 (CK2) is overexpressed in NSCLC and is correlated to a poor prognosis [7]. CK2 phosphorylation of its targets leads to the proliferation and morphology characteristic of NSCLC. Inhibitors of CK2 have incurred interest as potential anti-cancer drugs [8, 7].

After characterization, staging of the cancer is pivotal in determining the prognosis [9, 5]. Lung cancer is staged depending on the size of the tumor, proximity of the tumor to lymph nodes and whether the cancer has spread to different parts of the body. Depending on the stage of the cancer, proper therapy is chosen which ranges from surgical removal of lung portions, to chemotherapy and radiation therapy. However, where surgery is not an option, prolonged chemotherapy and radiation compromise the immune system of the patient, leaving the body susceptible to other diseases and infections. Thus novel and more effective therapeutic strategies are needed in the control of metastasis as well as growth of pulmonary cancers.

1.2 Flavonoids

In recent years, exercise regimes along with healthy diets have been shown to be effective in cancer prevention. Essential in healthy eating is a plant-based diet, particularly in fruits and vegetables containing substantial quantities of molecules that have chemopreventaitive potential to fight against cancer development [10]. These compounds include vitamins, trace elements, carotenoids, flavonoids and many other components of leafy, green vegetables [11]. Such diets contain high consumption of parsley and celery which are rich in polyphenolic compounds [12]. Polyphenolic compounds, called flavonoids, are comprised of approximately 5,000 substances defined chemically as having common phenlychromanone structure (C6-C3-C6), with multiple hydroxyl functional groups [13, 14]. Flavonoids are further classified into flavones, flavanols, isoflavones, flavonols, flavononones and anthocyanins (Table 1) based on structural features and varying positions of functional groups. Two major features of flavonoids contributing to their beneficial health properties are their anti-oxidant properties and capabilities to interact with proteins [15]. The structural similarity between purines and certain flavonoids leads to flavonoid inhibition of ATP dependant enzymes including kinases, topoisomerases and ABC transporters [16, 17]. Flavonoids with estrogen like structures, like the isoflavones, make for potent receptor agonists, with significant implications for cancer therapy [18].

The protective roles of bioactive molecules like flavonoids have been extensively noted in many studies. In the Zutphen study, cohorts of 878 men were followed for 25 years beginning in 1960, and monitored for incidence or mortality from all causes of cancer with the intake of 5 flavonoids; apigenin myricetin, quercetin, kaempferol and luteoin. The results showed that high intake of flavonoids from vegetables and fruits was inversely associated with risk of cancer [19]. In a more recent study, patients with resected colon cancer and polypectomy were divided into

Table 1. Common flavonoids including molecular structures as well as natural sources.

Flavonoid	Structure	Natural Sources
Flavones: Apigenin: R1=H, R2=OH Luteolin: R1=OH, R2=OH Chrysoeriol: R1=OCH_3, R2=OH	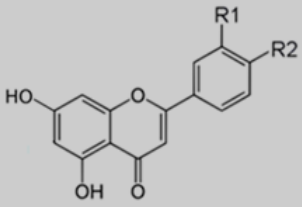	Celery, parsley, celery leaves, thyme, onions, chamomile, red pepper, lettuce, berries.
Flavonols: Kaempferol: R1 = H, R2 = OH Quercetin: R1 = OH, R2 = OH	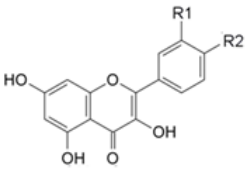	Black tea, olive oil, apple peels, kale.
Isoflanoves: Daidzein: R1 = H Genistein: R1 = OH	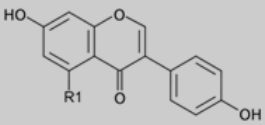	Soybeans, legumes , fava beans, psoralea.
Flavanones: Naringenin: R1 = H, R2 = OH Eriodictyol: R1 = OH, R2 = OH	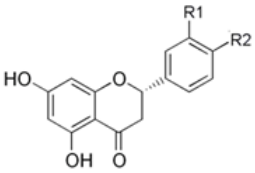	Citrus fruits, grape fruits. Tomatoes, mint, citrus fruits.
Anthocyanins: Pelargonidin: R1 = H, R2 = H Cyanidin: R1 = OH, R2 = H Delphinidin: R1 = OH, R2=OH	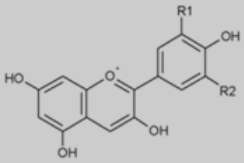	Aubergines, radishes. Red wine, beans, berries. Pomegranate, cherries, berries.

two groups, one receiving a flavonoid mixture (20 mg apigenin and 20 mg epigallocatechin-gallate) and a control group. Patients receiving the flavonoid diet had significantly lower rates of cancer recurrence, and reduced recurrence rate of neoplasia in patients with sporadic colorectal neoplasia [20]. These studies affirm that flavonoids contain attractive, therapeutic capabilities; however there is much to learn about the cellular mechanisms by which they function.

1.3 Apigenin

The flavone apigenin has incurred considerable interest for its attractive anti-inflammatory, anti-proliferative and anti-carcinogenic properties, however the underlying mechanisms by which it acts are poorly understood. Apigenin (Figure 1a), chemically 4',5,7,-trihydroxyflavone ($C_{15}H_{10}O_5$, MW 270.24), is also found naturally as biapigenin (Figure 1b) and is abundant is common in grapefruit, vegetables, parsley, onions, oranges, tea chamomile, and some seasonings [21,22]. The most abundant natural forms of apigenin are found in their glycoside form, where a sugar residue is conjugated to one of the hydroxyl groups (ex. apigenin-7-*O*-glucoside) and various acylated derivatives (Figure 1c,d) [23].

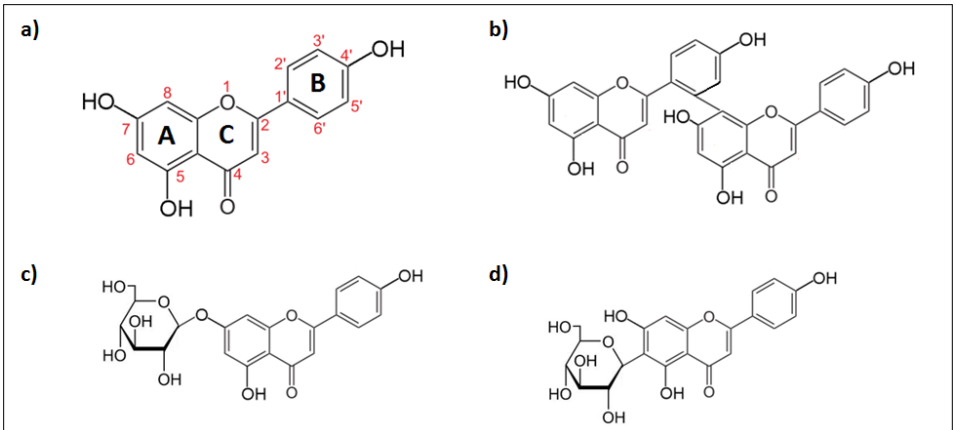

Figure 1. Molecular structure of apigenin and its natural derivatives a) Molecular structure of apigenin, numbering scheme and ring lettering. **b)** Molecular structure of biapigenin **c)** apigenin-7-*O*-glucoside **d)** apigenin-6-*C*-glucoside.

The interest in apigenin stems both from its attractive effects on cancerous cells and its low toxicity in comparison with other related flavonoids [24]. Some of the biological effects of apigenin come from the molecule's anti-oxidant and free radical scavenging abilities. Apigenin takes a protective role in murine studies were specimens were exposed to apigenin before carcinogenic insult [25]. Apigenin generates reactive oxygen species, causes loss of mitochondrial Bcl-2 expression, increases mitochondrial permeability, causes cytochrome c

release, and induces cleavage of caspase-3,-7,-8 and -9 which are crucial in the execution of programmed cell death, apoptosis [26]. Unlike its close predecessor naringenin, apigenin induces apoptosis in leukemia cells mediated by the activation of protein kinase C δ (PKC δ) [27]. Inhibition of protein kinase CK2, a serine-threonine kinase involved in cell cycle regulation by apigenin, involves the flavonoid in cell cycle regulation [28]. Apigenin is also a potent inhibitor of ornithine decarboxylase, an enzyme of the pyrimidine synthesis pathway heavily involved in tumor promotion. Further anti-carcinogenic abilities of apigenin were demonstrated with topical application of the flavonoid in dimethyl benzanthracene-induced skin tumors [29]. Other notable interactions of apigenin include telomerase [30] and fatty acid synthase [31] inhibition, matrix metalloproteinases [32], and suppression of cell cycle through aryl hydrocarbon receptor activity [33], all of which are relevant in different human diseases.

The role of the flavone to down-modulate pro-inflammatory cytokines implicates it in inflammatory diseases. Monocytes are produced daily in bone marrow and circulate in the blood for 24-48 hrs before undergoing apoptosis [34]. However, this apoptotic fate is halted by inflammatory stimuli [35]. Pro-inflammatory cytokines, such as TNFα (Tumor necrosis factor), and stimulatory signals such as lipopolysaccharide (LPS), a component of gram-negative bacteria cell wall, inhibit the apoptotic program by promoting monocyte survival [34, 35]. This prolonged survival contributes to the maintenance and onset inflammation. Monocyte evasion of apoptosis and differentiation to macrophages is also relevant in solid cancers where macrophage infiltration has been linked to tumor progression [36]. Our group showed that apigenin inhibits the production of pro-inflammatory cytokines by down-modulating the transcriptional activity of NF- κB in stimulated monocytes and in a mouse model of acute inflammation [37].

The ability of apigenin to interject in many important cellular functions and its potential to be utilized as a therapeutic in both cancer and inflammation compound the need to elucidate the mechanisms by which it acts. In working towards finding apigenin's mechanism of action, our lab used a phage-display breast cancer library, coupled with next generation sequencing and identified the heterogeneous nuclear ribonucleoprotein A2/B1 as a direct target of apigenin.

1.4 Heterogeneous Nuclear Ribonucleoproteins

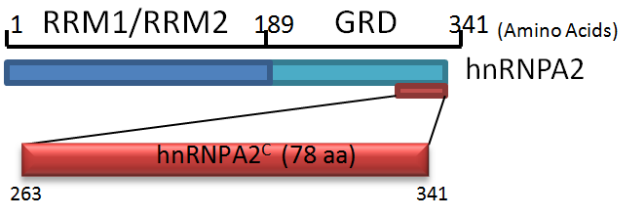

Figure 2. Heterogeneous nuclear ribonucleoprotein A2. Schematic representation of hnRNPA2, highlighting the general layout of most hnRNP molecules including the two RNA recognition motifs (RRM) and the glycine rich domain (GRD). The C-terminal, 78 amino acid portion shown (hnRNPA2^{C}) represents the part of the protein in the phage display.

Heterogeneous nuclear ribonucleoptoteins (hnRNPs) are amongst the most abundant RNA-binding proteins which associate with nascent pre-mRNAs, thereby complexing them into hnRNP particles [38]. The family consists of more than 20 major polypeptides, A1 to U, ranging in sizes of 34 to 120 kDa which in accord are responsible for mRNA metabolism [38]. All hnRNP proteins contain nuclear localization signal (NLS) and at least one N-terminal RNA recognition motif (RRM) and a C-terminal glycine-rich domain (GRD) (Figure 2). The C-terminal domain of the hnRNPs is crucial in mediating the protein's functional properties through regulation of protein-protein interactions with other hnRNPs. This form of regulation has been implicated in the alternative splicing of target mRNAs, thereby favoring one splice variant over another [39]. The hnRNPA/B subfamily have high levels of complimetarity in sequences, most significantly in their structural motifs. Human hnRNPs A1 and A2 exhibit approximately 80% homology in their RRM and 58% in their GRD [39, 40]. The family is encoded by 10 human genes which due to their sequence

complimentarily, are thought have arisen form one single RNA-binding protein by gene duplication [39].

1.4a Heterogeneous Nuclear Ribonucleoprotein A2

HnRNPA2 is the most abundantly expressed hnRNP proteins, compromising 60% of the protein family mass, along with hnRNPA1 [41]. Both proteins have been described to bind poly-nucleotides of dsDNA at regulatory elements including hormone response elements [41, 42]. However, the interaction of hnRNPA2 with RNA is much more established. HnRNPA2 has been shown to associate with the 21 nt hnRNPA2 response element (A2RE), or the derivative 11 nt (A2RE11) which is crucial in the transport of certain mRNAs to the cytoplasm in oligodendrytes and neurons [43-45]. The evolutionarily conserved A2RE sequences are also found in other transcripts, including; PRM2 (protein subunit of mitochondrial RNase P), MOBP81A (myelin-associated oligodendrocytic basic protein 81A), GABARα (GABA receptor α subunit), GFAP (glial fibrillary acidic protein, an intermediate filament), α-CaMKII (alpha-isoform of calcium/calmodulin-dependent kinase II) and ARC (activity-regulated cytoskeleton-associated protein) [44-47]. HnRNPA2 can also interact with A2RE-like sequences which are found in a region of overlap between the *vpr* and *tat* genes of the HIV-1 virus *in vitro* [48]. Further *in vitro* data show that apart from the A2RE and A2RE-like sequences, hnRNP A2 and its splice variant B1 bind UUAGGG sequences [49]. Microarray studies targeted at identifying downstream targets of hnRNPA2/B1 found a group of transcripts which did not contain A2REs, suggesting that hnRNPA2 may either associate directly with other unidentified RNA binding sequences or bind indirectly through associations with other hnRNPs [38]. The hnRNP A2 RNA-recognition motifs (RRMs) are both required for high-fidelity binding of the protein to RNA, as a single RRM has been observed to lose sequence recognition [50].

HnRNPA2 has also been implicated in chromosome maintenance and DNA replication. HnRNPA2 binds to SET oncoprotein, a key regulator of DNA replication, chromatin remodeling and gene transcription. It acts as an inhibitor of protein phosphatase 2A, an enzyme that regulates cell proliferatin and differentiation. The unfolding of tetraplex structures, which appears to be widespread across the human genome by hnRNPA2 and other hnRNPs may facilitate DNA replication [51, 52]. HnRNPB1 has also been shown to participate in DNA repair by associating with the DNA-dependant protein kinase (DNA-PK) complex, which mediates the repair of DNA double-strand breaks, by inhibiting its activity, whereas hnRNPA1 and A2 have no effect [53]. The association of hnRNPA2 with telomeric single-stranded repeat (TTAGGG) has been well documented. HnRNPA2 plays an important role in the protection of the telomeric repeat and not its complementary sequence from the degradation and hnRNP overexpression is implicated in telomere lengthening [54,55].

The broad functions of the hnRNPA2 protein also extend to gene transcription. HnRNPA2/B1 binds to promoter regions of *c-myc*, APOE, breast cancer 1 (BRCA1) and gonadotropin-releasing-hormone 1 (GnRH1) [56-59]. The exact role of hnRNPA2 as transcriptional activator or repressor has yet to be determined, but the mechanisms may be both direct and indirect. Pull-down assays using a glutathione s-transferase (GST) tagged p53 transcriptional activation domain detected hnRNPA2/B1, suggesting the possibility of A2/B1 forming a complex with p53, which is a multi-targeting transcription factor [38, 60, 61].

Splicing is an important process of mRNA maturation in which hnRNPs are involved. A study characterizing the requirement for a range of hnRNP proteins in alternative splicing of apoptotic genes has indicated that the splicing events controlled by hnRNP proteins varies between cell lines [62]. HnRNPs regulate pre-mRNA splicing by associating with exonic

splicing silencers (ESS) and intronic splicing silencers (ISS), interfering with 3' splice sites or promoting the use of more distal 5' splice sites [63]. The ability of hnRNPA2 to mediate alternative splicing of genes is crucial in the balance of normal and disease state within cells. This observation has lead to the investigation of hnRNPA2 mediated alternative splicing within certain cancers. Two recently characterized alternative splicing transcripts under hnRNPA2 control are pyruvate kinase and tumor protein p53 inducible nuclear protein 2 (TP53INP2). As described by David *et al*, pyruvate kinase (PK) has two isoforms which are differentially expressed. The PKM1 isoform promotes oxidative phosphorylation, while the embryonic PKM2 is expressed in growing cells and cancers. Human gliomas, with documented hnRNPA2 overexpression, preferentially express the PKM2 isoform due to the A2 repressive binding of flanking sequences of exon 9, which translates to the PKM2 isoform and a key requirement for tumor cell proliferation [64]. Likewise, TP53INP2 alternative splicing by hnRNPA2 was shown to be responsible for the migratory capabilities of ovarian carcinoma cells. HnRNPA2 knockdowns of the same cells showed reduced migration [65].

Therefore the concentration of hnRNPA2 weighs heavily on its function. It is no wonder then, that the overexpresssion and mislocalization of hnRNPA2 has been described in a multitude of cancers, including lung [66], breast [67], colon [40] and stomach carcinomas [68]. The overexpression of hnRNPA2/B1 in lung cancer has been investigated as an early detection biomarker in pre-cancerous, at risk patients [66]. HnRNPA2 has also been documented to interact with CK2, an interaction with implications for cell growth and migration that have yet to be fully understood [69]. With the current studies in our lab identifying hnRNPA2 as a previously undescribed target of the flavone apigenin, we explore the beneficial possibilities of the apigenin-hnRNPA2 interaction on lung cancer cell lines.

The goals of this project were to further study the interaction of apigenin and other biologically active flavonoids with hnRNPA2, as well as investigate the physiological effects of the flavone-protein interaction on lung cancer. With the use of a FRET nanosensor, we found that apigenin and other similarly structured flavonoids bind the hnRNPA2 protein. The treatment of lung cancer cell lines with apigenin decreased their migratory abilities but did not have an effect on the expression levels of hnRNPA2 at the transcriptional or translational level. Our work elucidates the mechanistic pathway of apigenin in lung cancer and provides evidence for the potential target of novel anti-cancer and anti-inflammatory therapeutics.

2. Materials and Methods

2.1 Plasmid Construction

Generation of the fluorescence indicator proteins (FLIP) constructs was accomplished using human hnRNPA2^c cDNA, amplified by PCR from pET9c-hnRNPA2 vector using forward primer PAO-378 (5'-AAGGAAAAAAGCGGCCGCCGGTACCGGCAACCAGGGTG-3') and reverse primer PAO-379 (5'-TTATAGGCGCGCCCACTAGTCTATCGGCTCCTC-3') to generate clones with proper restriction sites to be used in downstream reactions. The PCR reactions were carried out with 50 ng of DNA template, 25 pmol forward and reverse primers, 3 mM $MgCl_2$, 500 µM dNTP, 1x High Fidelity PCR Buffer (Invitrogen, Carlsbad, CA), 1 unit High Fidelity Taq polymerase (Invitrogen, Carlsbad, CA) and dH_2O. The PCR was run with 35-cycles of 30 sec at 95°C, 30 sec at 58°C, and 1 min at 72°C. PCR fragments were digested first with restriction enzyme Not 1 (New England Biolabs, Ipswich, MA), 1X bovine serum albumin (BSA), 1X NEB Buffer 3 (New England Biolabs, Ipswich, MA), and dH_2O for 20 h at 37^{o}C. The digestion products were purified utilizing PCR Purification kit (Invitrogen Carlsbad, CA)and then digested with Asc1 (New England Biolabs, Ipswich, MA), 1X BSA (New England Biolabs, Ipswich, MA), 1X Buffer 4 (New England Biolabs, Ipswich, MA), and dH_2O for 3 h at 37^{o}C.

Simultaneously, four micrograms of pENTR/D-TOPO vector was digested with Not1 and Asc1 (New England Biolabs, Ipswich, MA), 1X BSA (New England Biolabs, Ipswich, MA), 1X Buffer 4 (New England Biolabs, Ipswich, MA), and dH_2O for 20 h at 37^{o}C. The digestion was combined with DNA loading buffer 6X (.25% bromophenol blue and 30% glycerol in H_2O) and ran on a 1% agarose gel (1 g agarose/ 100 ml 1x Tris-Acetate EDTA Buffer) containing 0.2 µg/ml ethidium bromide to stain the DNA. One kb plus DNA ladder was loaded alongside the

sample to verify the proper size of the fragments. The gel was run for 40 min at 100 V. The properly cut pENTR/D-TOPO vector, as determined by size, was excised from the gel and purified using the PureLink gel extraction kit (Invitrogen, Carlsbad, CA).

The hnRNPA2^{c} clones were ligated into the cut pENTR/D-TOPO vector using 50 ng hnRNPA2^{c} insert and 50 ng vector, 1X ligation buffer (Roche Basel, Switzerland), autoclaved H_2O and T4 ligase in a total volume of 10 µl. The ligation was incubated at room temperature for 2 h and transformed into MAX Efficiency *Stbl2*™ competent cells (Invitrogen Carlsbad, CA). Stbl2 cells were chosen to confront the problematic nature of the multiple repeats in the hnRNPA2^{c} sequence. Colonies were picked and screened using enzymes XhoI and SpeI (New England Biolabs, Ipswich, MA).

Positive clones where used in a recombination reaction to move the hnRNPA2^{c} insert into the pFLIP vector. Using the homologous recombination sites on the pENTR/D-TOPO vector and the His-tagged pFLIP vector, Gateway LR Clonase Kit was used to recombine the hnRNPA2^{c} fragment into the FLIP construct. The recombination reaction was transformed into MAX Efficiency *Stbl2*™ competent cells (Invitrogen Carlsbad, CA). Selectivity was provided by growing cells on Ampicillin containing plates as that is the resistance provided by the pFLIP vector. FLIP vectors that did not recombine were eliminated by the ccdB toxic gene contained within the recombination sites that should have been recombined out of the pFLIP vector. Screening was performed through restriction digestion and positive closes were re-transformed into BLR (DE) cells for protein expression. The pFLIP- hnRNPA2^{c} biosensor was created with four different fluorescence protein combinations (Table 2). pFLIP vectors were a generous gift of Dr. Wolf Frommer.

To create different FLIP- hnRNPA2^{c} with improved FRET capabilities, the N-terminal and C-terminal linkers between the fluorescent proteins and the hnRNPA2^{c} fragment (Figure 5) were preferentially digested out, the DNA fragments purified and then religated. In order to remove the N-terminal linker, a restriction digestion was performed using KpnI (New England Biolabs, Ipswich, MA) 1X bovine serum albumin (BSA), 1X NEB Buffer 1 (New England Biolabs, Ipswich, MA), and dH_2O for 3 h at 37^{o}C. To remove the C-terminal linker, SpeI restriction enzyme was used with the same restriction set up and to remove both linkers, the restriction digestion was performed with both KpnI and SpeI simultaneously. All fragments were purified using PureLink gel extraction kit (Invitrogen, Carlsbad, CA) after resolution with 1% agarose gel. The fragments were then ligated using 50 ng hnRNPA2^{c} insert and 50 ng vector, 1X ligation buffer (Roche Basel, Switzerland), autoclaved H_2O and T4 ligase in a total volume of 10 µl. The ligation was incubated at room temperature for 2 h and transformed into MAX Efficiency *Stbl2*™ Competent cells (Invitrogen Carlsbad, CA). After screening for positive clones through restriction analysis, positive clones were transformed into BLR(DE)LysS cells for protein expression.

2.2 Induction & Bacterial Cell Lysates

To test the fluorescence resonance energy transfer (FRET) of the FLIP- hnRNPA2^{c} nanosensors, inductions were performed to do FRET experiments using bacterial lysates. Single colonies of BLR(DE)LysS cells containing appropriate pFLIP-hnRNPA2^{c} constructs were picked and grown in 200 ml of LB Broth containing ampicillin (100 µg/ml), tetracycline (10 µg/ml) and chloroamphenicol (100 µg/ml). Cultures were grown to an optical density of 0.5 A_{600} at 37^{o}C and then induced for two hours at 30^{o}C using 1 mM isopropyl 1-thio-β-D-galactopyranoside (IPTG, Gold Biotechnology, St. Louis, MO). Cells were harvested at 6,000 g for 5 min and washed in 10

ml non-sterile phosphate buffered saline (PBS). Pellets were lysed by sonication (Duty cycle 30%, Output 5, 5 x 10 pulses) in Tris buffer (20 mM, pH 8) containing protease inhibitors DTT (1 mM), PMSF (0.1 mM), and Clap (2 mg/ml of the protease inhibitor cocktail containing chymostatin, leupeptin, antipain and pepstatin). Lysates were then centrifuged 15 min at 13,000 rpm and the supernatant was separated from the pellet. Protein content in the supernatant was quantified by SDS-PAGE (12% acrylamide) using a bovine serum albumin (BSA) standard curve and visualized through Coomassie blue staining.

2.3 Protein Purification

His-tagged CFP-hnRNPA2^{c}-YFP protein was obtained through the induction of 1L LB Broth cultures as previously described. Bacteria was resuspended in 10 ml Tris buffer (20 mM, pH 8) with protease inhibitors and lysed by sonication (refer to **Induction & Bacterial Cell Lysates** section). Lysates were centrifuged at 13,000 rpm for 10 min and the supernatant separated from the pellet. The supernatant was combined with 250 µl of 50% slurry nickel beads (Ni^{+}-NTA-superflow, Qiagen) and incubated at 4^{o}C for 2 h on a rocker. The mixture was loaded into a previously equilibrated column and washed three times with 1 ml of the Tris buffer. The protein was eluted with discontinuous imidazole gradient (20-50 mM). Elution fractions containing the CFP-hnRNPA2^{c}-YFP proteins were dialyzed in 20 mM Tris buffer, pH 8 for 6 h at 4^{o}C, in a 1:500 dilution.

2.4 Fluorescence resonance energy transfer (FRET) Assays

The ability of the different FLIP-hnRNPA2^{c} proteins to perform the energy transfer was screened using lysates. In a 96-well plate, 199 µl of extract were incubated with 1 µl of diluent dimethyl sulfoxide (DMSO) of apigenin concentrations from 1-100 µM. Emission spectra of the

FLIP-hnRNPA2^{c} was determined using spectrofluorometer plate reader (FlexStation3, Molecular Devices) by exciting the N-terminal Cyan fluorescent protein (Table M1,) and recording emission over the range of 460nm-600nm. FRET was determined as the intensity of the fluorescence emission of the peak corresponding to the C-terminal fluorescent protein (530 nm) divided by the intensity of the fluorescence of the N-terminal fluorescent protein (480 nm). The reaction was incubated at 37^{o}C and time points were taken at 0 h, without flavonoid treatment and then at 1 h and 24 h with flavonoid treatment. The ratios of C-terminal fluorescence protein peak emission (λ_{emis}) divided by N-terminal λ_{emis} were calculated and graphed to represent the change in FRET of the nanosensor protein in response to flavonoid treatment. CFP-hnRNPA2^{c}-YFP proteins which showed promising FRET capabilities were determined, and the FRET analysis was repeated using purified protein nanosensor with the previously described set up. Incubation at 37^{o}C for 3 h was used for analysis of purified protein nanosensor, after previous work performing a time course was showed the 3 h time point representing the best results.

Table M1. Excitation and emission of fluorescent proteins.

Fluorescent Protein	**λ_{ext}**	**λ_{emis}**
Cyan Fluorescent Protein (CFP)	405nm	480nm
Yellow Fluorescent Protein (YFP)	485nm	530nm
Green Fluorescent Protein (GFP)	395nm	510nm
monomeric Kusabira orange (mKO)	510nm	570nm

2.5 Dissociation Constants

Dissociation constants (K_D) of the flavonoid-protein interactions were calculated by fitting the YFP/CFP ratio curves to the equation of the binding of a ligand to a protein:

$$S = (r - R_{min})/(R_{max}-R_{min}) = [L]_{bound}/[P]_{total} = n[L]/(K_D + [L])$$

where S is saturation; [L] is ligand concentration; $[L]_{bound}$ is concentration of bound ligand; n is number of equal binding sites; $[FLIP]_{total}$ is total concentration of FLIP nanosensor; r, ratio; R_{min} is minimum ratio in the absence of ligand; and R_{max} is maximum ratio at saturation with ligand [17]. Saturation curves were obtained and K_D determined by non-linear regression with the aid of GraphPad Prism. Statistical significance between means in FRET experiments were determined by one-way ANOVA.

2.6 Tissue Culture & Treatment

A549, H1703, H1299 and H2009 (American Type Culture Collection (ATCC) Manassas, VA USA) cells were cultured in RPMI (A549) or DMEM (H1703, H1299 and H2009) and maintained in a modified atmosphere of 5% CO_2 with 10% heat inactivated bovine serum (FBS), 100 U/ml penicillin and 100 µl/ml streptomycin (P/S; BioWhittaker, Walkersville, MD). 5 x 10^5 cells were seeded in 1 ml media 16 h before flavonoid treatment. Cells were treated with 0, 1, 10 and 50 µM of flavonoid or diluent DMSO for 24 h. Cells were collected by centrifugation at 1200 rpm for 5 min, washed in phosphate buffered saline (PBS) and were used for either protein or transcriptional analysis.

2.7 RNA Isolation & Transcript Analysis

RNA isolation was performed using the Trizol method. Flavonoid treated mammalian cells were pelleted and resuspended in 0.5 ml of Trizol (Invitrogen). One hundred µl of chloroform was added to the samples, inverted vigorously and incubated at room temperature for 2-3 min. The samples were centrifuged at 12,000 rpm for 15 min at 4^{o}C to resolve the different components of the cells (pink bottom layer representing protein and membrane, white interface containing DNA and the clear top layer containing RNA). The top RNA layer was extracted, placed in a new tube and 250 µl of isopropanol were added to precipitate RNA. Tubes were inverted and incubated at room temperature for 10 min after which samples were centrifuged at 12,000 rpm for 10 min at 4^{o}C. The gel-like pellet was washed in 500 µl of 75% ethanol and centrifuged at 12,000 rpm for 5 min at 4^{o}C. Pellet was resuspended in 50 µl of diethyl dicarbonate (DEPC) treated water (DEPC-H_2O).

Isolated RNA was used to create cDNA for downstream experiments with ThermoScript RT-PCR System (Invitrogen). Two hundred ng of RNA in 2 µl were added to 0.4 µl Oligo(dT), 0.4 µl Random Hexomers, 1 µl dNTPs and 4.25 µl DEPC-H_2O, then incubated at 65^{o}C for 5 min. To the reaction mix was added 4 µl 5X cDNA Synthesis Buffer, 1 µl DTT, 0.1 µl RNaseOUT, 0.1 µl ThermoScript RT (15 U/ µl) and 6.25 µl DEPC-H_2O. The reaction was incubated at 50^{o}C for 60 min. Transcriptional expression analysis was carried out through Real-Time PCR of previously manufactured cDNA. Ten µl SybrGreen (Applied Biosystems) PCR master mix was combined with 2 µl cDNA and 250 nmol/L of primers (Table M1) in a total reaction mix of 20 µl.

Table M2. List of primers utilized for Real-Time PCR.

PAO-416	hnRNPA2	5'-GGCTACGGAGGTGGTTATGA-3'	Forward
PAO-417	hnRNPA2	5'-ACCCCCAAAGTTTCCACTCT-3'	Reverse
PAO-296	rRNA 18s	5'-GTAACCCGTTGAACCCCATT-3'	Forward
PAO-297	rRNA 18s	5'-CCATCCAATCGGTAGTAGCG-3'	Reverse

2.8 Western blot

Extracts from 1 x 10^6 cells were incubated with Lysis Buffer B (Ingredients: 40 mM Hepes, 0.3 M NaCl, 3 mM $MgCl_2$, 0.3 mM EGTA, 0.1% Tween, 50 mM sodium fluoride, 10 mM sodium glycerophosphate, 5 mM sodium pyrophosphate, 1 mM orthovanadate, 1 mM DTT, 0.1 mM PMSF, and 2 µg/ml Clap) for 20 min on ice and vortexed 5 sec every 5 min. Lysates were sonicated (Duty cycle 30%, Output 5, 3 x 5 pulses) and centrifuged 12,000 rpm for 10 min at 4^{o}C. Supernatant was extracted and quantified by Bradford assay. Equal amounts of protein were loaded and resolved by SDS-PAGE on 12% acrylamide gel at 150 V for 80 min. Proteins were transferred to Protran Nitrocellulose Blotting Membranes (0.2 µm, Whatman, USA) for 70 min at 100 V utilizing transfer buffer (25 mM Tris, pH 8.3, 192 mM glycine, 20% methanol). Membranes were blocked using 5% milk in TBS (10 mM Tris-HCl, 150 mM NaCl, 0.05% Tween, pH 7.6) and incubated with anti-hnRNPA2 primary antibody (1:2000 Maker/Brand) to detect hnRNPA2 (36 kDa) 16 h at 4^{o}C. Anit-mouse secondary antibody conjugated to horseradish peroxidase (1:6000, GE, Piscataway, NJ) was added and incubated for 1 hr at rt. Proteins were visualized by autoradiography (Amersham Pittsburgh, PA).

2.9 Bradford Assay

Bio-read protein assay reagent 5X (Bio-Rad, Hercules, CA) was diluted to 1X and added to standards of 0, 2, 4, 6, and 8 µg BSA to a total 200 µl. Absorbance was measured and used to plot a standard curve. One µl of protein sample was added to 199 µl of Bradford reagent, absorbance measurements taken at 595 nm. To quantify the protein, a standard cure was generated using known increasing concentrations (100 – 1600 µg) of bovine serum albumin (BSA) and used to calculate the protein concentration.

2.10 Migration Assay

A549, H1703, H1299 and H2009 lung cancer cell lines American Type Culture Collection (ATCC) Manassas, VA USA) were cultured in RPMI (A549) or DMEM (H1703, H1299 and H2009) containing 10% heat inactivated bovine serum (FBS), 100 U/ml penicillin and 100 µl/ml streptomycin (P/S; BioWhittaker, Walkersville, MD). 5×10^5 cells were seeded 16 hours before treatment in twelve-well plates. The monolayer of cells attached to the bottom of the plate were scratched with a pipette tip, and the detached cells were removed with a PBS wash [70]. Media was then added containing the apigenin treatment (0, 1, 10, and 50 µM), and the cultures were incubated in the modified atmosphere of 5% CO_2 at 37 ^oC for 24 h at which point the invasive cell migration was photographed at 10x magnification (OlympusIX50 Microscope, Olympus QColor3 Camera, and QCapture Pro 6.0 Software).

3. Results

3.1 Generation of a Flavonoid Nanosensor

To identify direct targets of apigenin, the flavonoid was immobilized to PEGA (polyethyleneglycol-polyarcylamide) resin beads which were used to screen a phage display breast cancer library. One of the targets identified by pahge display was the heterogenous nuclear ribonucleoprotein A2 (hnRNPA2). After several molecular tests, including pull-downs using GFP-hnRNPA2 proteins, we were able to show that hnRNPA2 binds to apigenin. In order to study the interaction of apigenin with hnRNPA2 a genetically encoded flavonoid nanosensor using fluorescence resonance energy transfer (FRET) was developed. FRET based nanosensors have previously been used to monitor small molecule to protein interactions [71]. The rationale for developing a biosensor is that a nanosensor would allow us to also survey a variety of other biologically active flavonoids, to see if they also functioned through hnRNPA2. FRET nanosensor technology has previously been utilized in studies monitoring glucose uptake within cells [71]. In this case, a glucose binding protein was flanked by two fluorescent proteins, which upon the binding of glucose would increase the rate of energy transfer between the two fluorescent constituents. This energy change is monitored and quantified for analysis [72]. The nanosensor is capable of generating highly useful information based on the concentration of ligand, making it possible to not only verify a small molecule to protein interaction but also obtain dissociation constants that describe the interaction.

There are certain molecular qualifications that need to be considered in the development of a FRET nanosensor. The first qualification concerns the ability to observe the energy transfer between the C-terminal and N-terminal fluorescent proteins flanking the target protein, in our

case the apigenin binding domain of hnRNPA2 (hnRNPA2^{c}) defined by pull-downs using different domains of hnRNPA2 (Figure 2). Secondly, the fluorescent resonance energy transfer would change as ligand concentration is increased. For the first property, the fluorescent proteins must be in the proximity of 5-10 nm to allow the energy transfer to occur. For the second property, the application of apigenin, through binding to hnRNPA2^{c}, would cause a conformational change in the protein that would change the efficiency of energy between the two flanking fluorescent proteins (Figure 3).

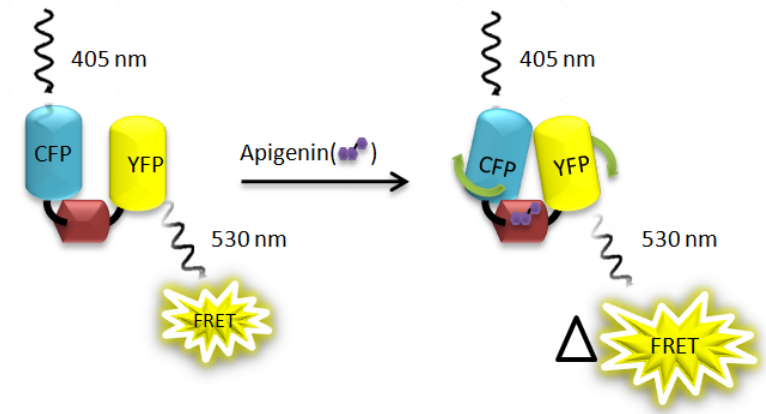

Figure 3. FRET nanosensor Schematic representation of the fluorescence energy transfer required for the nanosensor. The N-terminal cyan fluorescent protein (CFP) is excited at 405 nm and emits at 480 nm, which is the excitation of yellow fluorescent protein (YFP). YFP then emits energy at 530 nm, this energy transfer is called FRET. Treatment and binding of apigenin to hnRNPA2 causes a conformational change in the protein causing the fluorescent proteins to move closer together, improve energy transfer, and ultimately have a higher FRET ratio.

The first step in the generation of the apigenin nanosensor was to clone the fragment identified by the phage display approach that interacts with apigenin (named throughout the text as hnRNPA2^{c}) into an entry vector. For this purpose, the human hnRNPA2^{c} fragment was amplified through PCR and ligated into pENTR/D-TOPO entry vector. All attempts using traditional methods of cloning into the pENTR/D-TOPO entry vector were unsuccessful. To overcome these technical difficulties, a normal ligation approach was used. The fluorescence indicator protein (FLIP) nanosensor was generated using human hnRNPA2^{c} (Figure 2) cDNA,

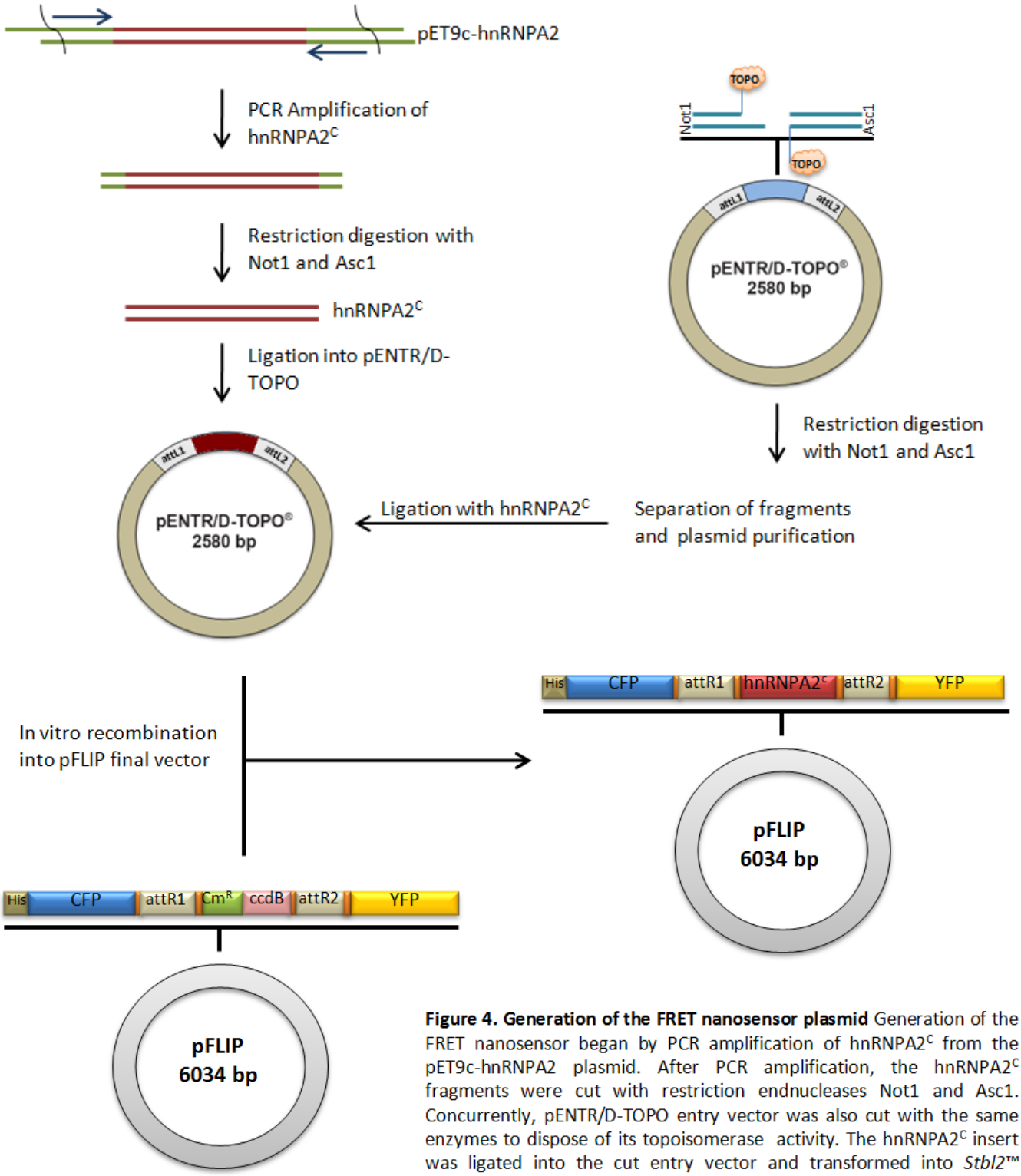

Figure 4. Generation of the FRET nanosensor plasmid Generation of the FRET nanosensor began by PCR amplification of hnRNPA2^{C} from the pET9c-hnRNPA2 plasmid. After PCR amplification, the hnRNPA2^{C} fragments were cut with restriction endnucleases Not1 and Asc1. Concurrently, pENTR/D-TOPO entry vector was also cut with the same enzymes to dispose of its topoisomerase activity. The hnRNPA2^{C} insert was ligated into the cut entry vector and transformed into *Stbl2*™ Competent cells. After screening and plasmid purification, a recombination reaction was used to place the hnRNPA2^{C} insert into its final vector, pFLIP, in between the two fluorescent proteins.

amplified by PCR from pET9c-hnRNPA2 vector using forward and reverse primers PAO-379 and PAO-378 respectively and proper restriction enzyme sites Not1 and Asc1 were introduced (Figure 4). PCR fragments were digested first with the restriction enzyme Not1, purified utilizing PCR Purification kit (Invitrogen Carlsbad, CA) and then digested with Asc1 to provide a fragment of 234 bp for subsequent ligation.

Simultaneously, the pENTR/D-TOPO vector was digested with Not1 and Asc1. Cut vector was separated from uncut by agarose gel electrophoresis and the properly cut band was excised from a gel and purified (See Materials and Methods). The hnRNPA2^{c} clones were ligated into the cut pENTR/D-TOPO vector and transformed into MAX Efficiency *Stbl2*™ Competent cells. Stbl2 cells were chosen to confront the problematic nature of the multiple repeats in the hnRNPA2^{c} sequence. Stbl2 genome is ideal to use for repetitive inserts due it mutations in its recombinase (*recA1*), along with a unique set of genetic markers specialized for direct repeat and retroviral sequences. Colonies were selected, DNA purified, and clones containing the fragment of interest were screened using enzymes Not1 and EcoRV allowing us to assess proper insertion and directionality.

Positive clones where used in a recombination reaction to clone the hnRNPA2^{c} insert into the pFLIP vector. Using the homologous recombination sites (attL1 and attL2) on the pENTR/D-TOPO vector and the His-tagged pFLIP (attR1 and attR2) vector, Gateway LR Clonase Kit was used to recombine the hnRNPA2^{c} fragment into the FLIP construct. The recombination reaction was again transformed into MAX Efficiency *Stbl2*™ competent cells. Selectivity for the recombination was provided by growing cells on ampicillin plates, as that is the resistance provided by the pFLIP vector. pFLIP vectors that did not recombine were eliminated by the *ccdB* (coupled cell division B) toxic gene contained between the recombination sites that should have

been recombined out of the pFLIP vector (Figure 4). After DNA purification, screening was performed through restriction digestion enzymes XhoI and SpeI. Positive clones were re-transformed into BLR(DE)LysS, which also have an optimized genome for repetitive inserts, for protein expression.

To create different FLIP-hnRNPA2^{c} proteins with improved FRET capabilities, the N-terminal and C-terminal linkers (corresponding to the recombination sequences attR1 and attR2) flanking the hnRNPA2^{c} insert were preferentially digested out, the DNA fragments purified and then re-ligated (Figure 5a). In order to remove the N-terminal linker, a restriction digestion was performed using KpnI (Figure 5b). SpeI restriction enzyme was used to remove the C-terminal linker and to remove both linkers, the restriction digestion was performed with both KpnI and SpeI simultaneously. After digestion with the specific enzymes, the fragments were separated by gel electrophoresis (Figure 5c), purified and re-ligated to yield a total of three combinations of linkers with distinct FRET capabilities. Removal of the N-terminal linker was designated as pFLIP2-2-hnRNPA2^{c}, C-terminal excision as pFLIP2-1-hnRNPA2^{c}, and excision of both designated pFLIP2-3-hnRNPA2^{c}. The hnRNPA2^{c} fragment was inserted in between three combinations of fluorescence proteins to increase the likelihood of generating a properly functioning nanosensor (Table 2).

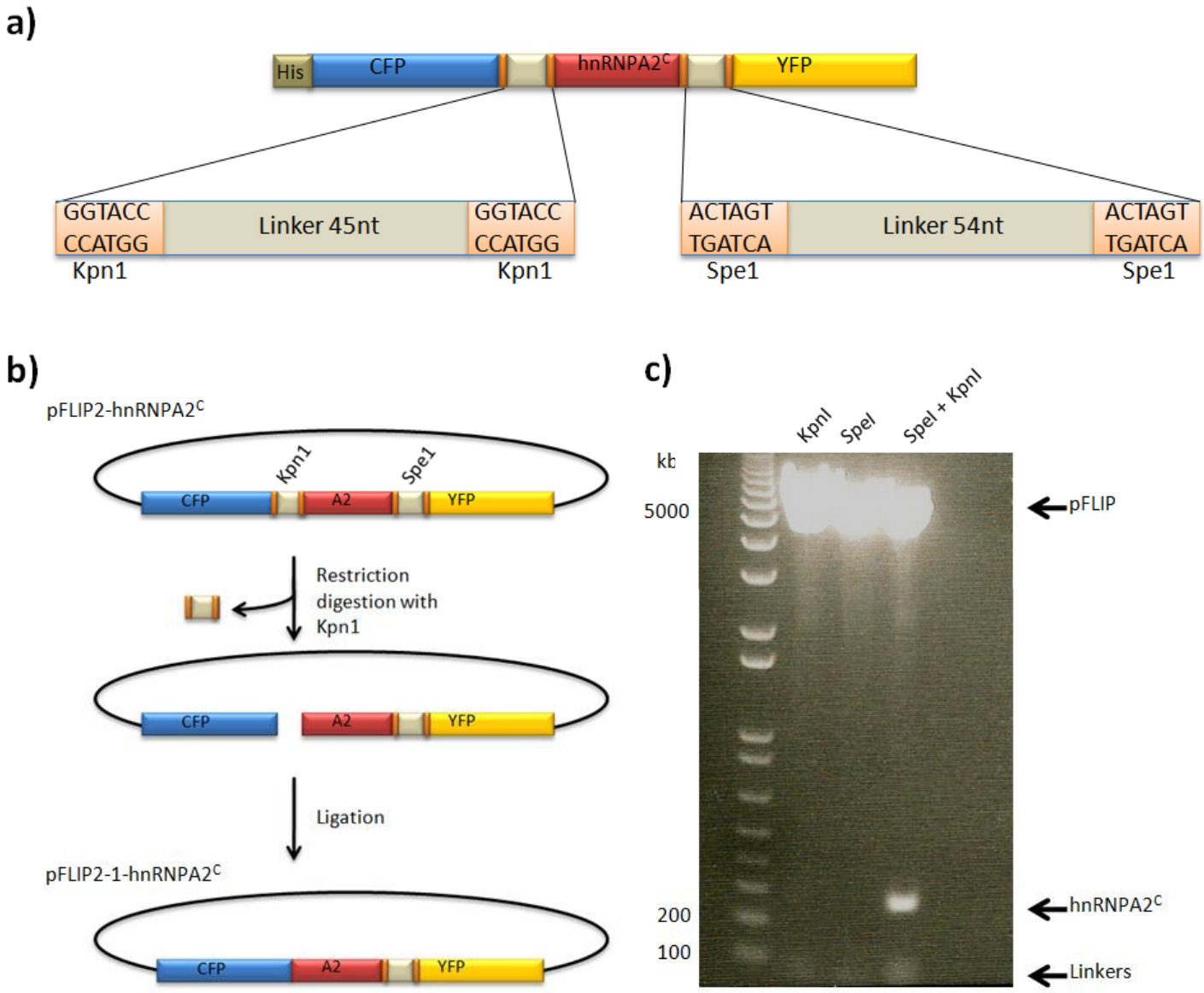

Figure 5. Alternate plasmid constructed for the nanosensor the improve FRET a) Representation of the final nanosensor coding region of the pFLIP plasmid. The figure highlights the N-terminal His tag as well as the two linker sequences, corresponding to the recombination sites, and the flanking restriction digestion sites of each (Kpn1 and Spe1 respectively). **b)** Schematic of the methods taken to remove the N-terminal linker so as to improve the FRET capabilities of the nanosensor. The DNA was cut with Kpn1, resolved on a gel and then re-ligated. After removal of the N-terminal linker, the construct was called pFLIP2-1-hnRNPA2^{C}. **c)** Agarose gel showing the plasmid cut with either Kpn1, Spe1 or both enzymes simultaneously. All three lanes show the digested linkers below 100 bp, and the hnRNPA2

Table 2 . List of all clones generated for the FRET-based flavonoid nanosensor.

FLIP	Construct	AB Number
pFLIP2-hnRNPA2^{c}		AB731
pFLIP2-1-hnRNPA2^{c}		AB739
pFLIP2-2-hnRNPA2^{c}		AB740
pFLIP2-3-hnRNPA2^{c}		AB741
pFLIP3-hnRNPA2^{c}		AB732
pFLIP4-hnRNPA2^{c}		AB733
pFLIP4-1-hnRNPA2^{c}		AB750
pFLIP4-2-hnRNPA2^{c}		AB751

3.2 Nanosensor Screening and Protein Expression

In order to determine the FRET capabilities of the FLIP-hnRNPA2^{c} clones, proteins were induced from bacteria as previously described by Fehr *et al* with some modifications [7]. An advantageous feature of our nanosensor clones is that their FRET capabilities were shown to be functional in bacterial lysates. First we determined the optimal conditions for FLIP-hnRNPA2^{c} proteins. Single colonies of BLR(DE)LysS cells containing appropriate pFLIP-hnRNPA2^{c} expression clone were grown with appropriate antibiotics overnight. Cultures were induced for 1, 2, and 3 h at 30^{o}C using isopropyl 1-thio-β-D-galactopyranoside (IPTG). Results from these studies indicated that inductions performed at 37^{o}C over a 1, 2, and 3 h time course yielded a protein that was degraded. However, inductions performed at 30^{o}C over the same time points did not show degradation of the protein (Figure 6a). Next, we evaluated the solubility of the protein

induced. For this purpose, inductions were performed at 30^{o}C for 1, 2, and 3h. Bacteria pellets were lysed and centrifuged to obtain the bacterial supernatant and pellet fractions. The pellet was resuspended in an equivalent volume to the supernatant and fractions of both were loaded onto a SDS-PAGE gel (Figure 6b). Gels stained with Commassie showed a polypeptide of approximately 64 kDa that was primarily found in the pellet or insoluble fraction. While we observed an increase in the expression of the FLIP proteins over the 3 h period, the amount found in the soluble fraction remained similar during all times of induction. Therefore, taken with the results from the different temperature studies, we determined that the optimal conditions to obtain soluble pFLIP-hnRNPA2^{c} were for 2 h of IPTG induction at 30^{o}C. Next, using the conditions of induction determined, the different pFLIP clones were induced and the soluble fraction of protein quantified by SDS-PAGE using a standard curve generated by loading increasing concentrations of bovine serum albumin (BSA and visualized through Coomassie blue staining (Figure 6c).

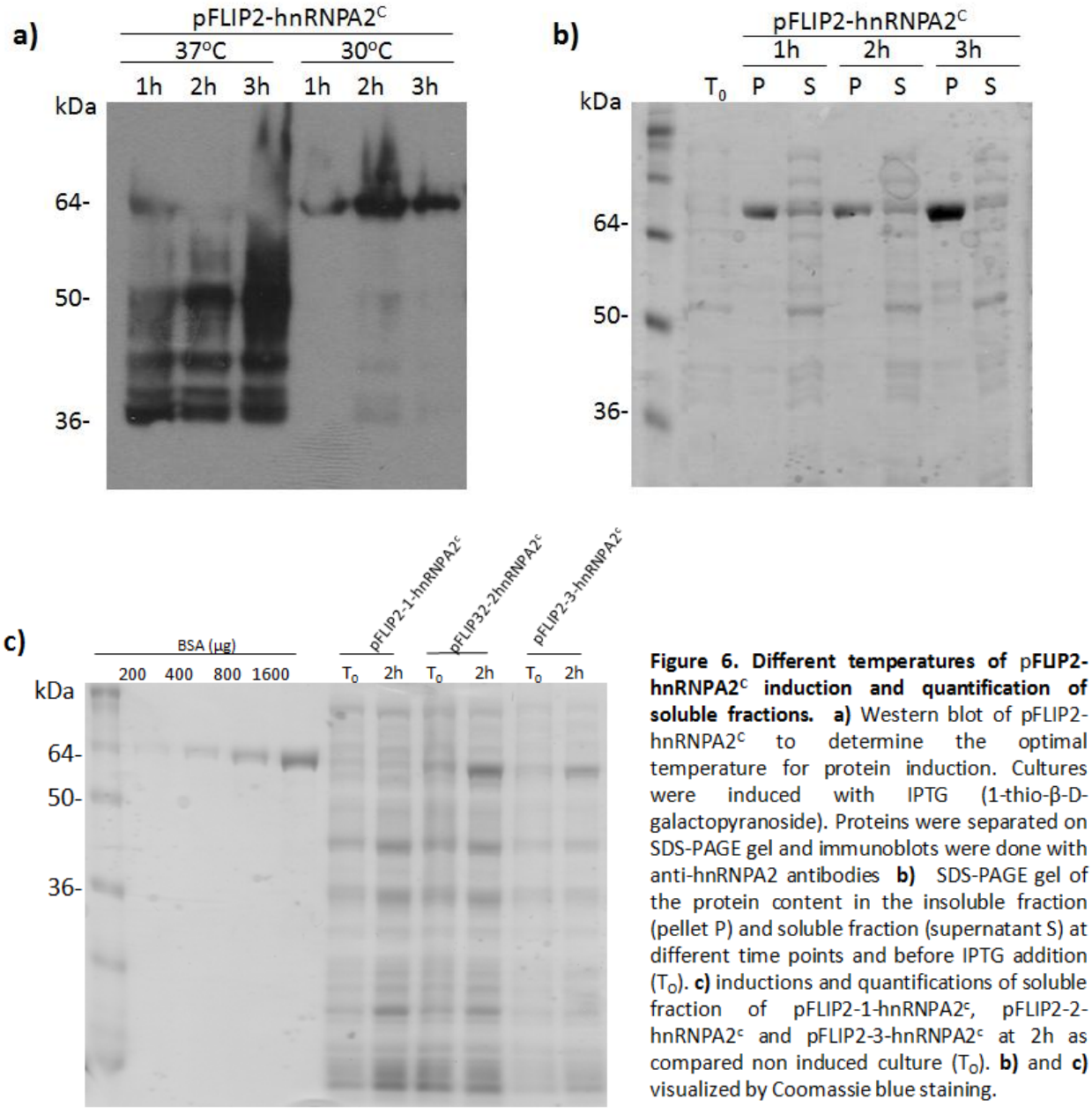

Figure 6. Different temperatures of pFLIP2-hnRNPA2^C induction and quantification of soluble fractions. **a)** Western blot of pFLIP2-hnRNPA2^C to determine the optimal temperature for protein induction. Cultures were induced with IPTG (1-thio-β-D-galactopyranoside). Proteins were separated on SDS-PAGE gel and immunoblots were done with anti-hnRNPA2 antibodies **b)** SDS-PAGE gel of the protein content in the insoluble fraction (pellet P) and soluble fraction (supernatant S) at different time points and before IPTG addition (T_O). **c)** inductions and quantifications of soluble fraction of pFLIP2-1-hnRNPA2^c, pFLIP2-2-hnRNPA2^c and pFLIP2-3-hnRNPA2^c at 2h as compared non induced culture (T_O). **b)** and **c)** visualized by Coomassie blue staining.

The ability of FLIP-hnRNPA2^{c} proteins to perform the energy transfer was tested. For this purpose, lysates of bacteria expressing the clones listed on Table 2 were incubated with 1 µl of diluent dimethyl sulfoxide (DMSO) or apigenin at concentrations ranging from 1-25 µM. Emission spectra of the FLIP-hnRNPA2^{c} was determined using spectrofluorometry by exciting the N-terminal fluorescent protein (Table 3) and recording emission over the range of 460-600 nm. FRET was determined as the intensity of the fluorescence emission of the peak corresponding to the C-terminal fluorescent protein (ex. YFP: 530 nm) divided by the intensity of the fluorescence of the N-terminal fluorescent protein (ex. CFP: 480 nm). The reaction was incubated at 37^{o}C and time points were taken at 0 h, without flavonoid treatment and then at 1 and 24 h (results shown at 1h) with flavonoid treatment. The ratios of C-terminal fluorescence protein peak emission (λ_{emis}) divided by N-terminal λ_{emis} were calculated and graphed to represent the change in FRET of the nanosensor protein in response to flavonoid treatment (Figure 7). Of the eight constructs generated, only four possessed the first property of a nanosensor which is efficient energy transfer between the fluorescent proteins (FLIP-2-hnRNPA2^{c}, FLIP-2-2-hnRNPA2^{c}, FLIP-2-3-hnRNPA2^{c} and FLIP3-hnRNPA2^{c}). Of those, only FLIP-2-3-hnRNPA2^{c} (Figure 7), showed a significant change in FRET ratio with increasing apigenin concentrations. Thus, we focused on this construct for subsequent experiments.

In order to augment the change in FRET ratio, we increased the concentrations of apigenin (0, 1, 5, 10, 25, 50, 100 µM), as well as recording FRET at 0, 1, 3, 12 and 24 h. These studies improved the variability observed with bacterial lysates allowing more consistent results. With the new conditions, we satisfied the second qualification of the FRET nanosensor which was a dose dependant change in FRET with increasing apigenin concentration (Figure 8). This suggested that the 3h incubation allowed for sufficient interaction of the protein and ligand,

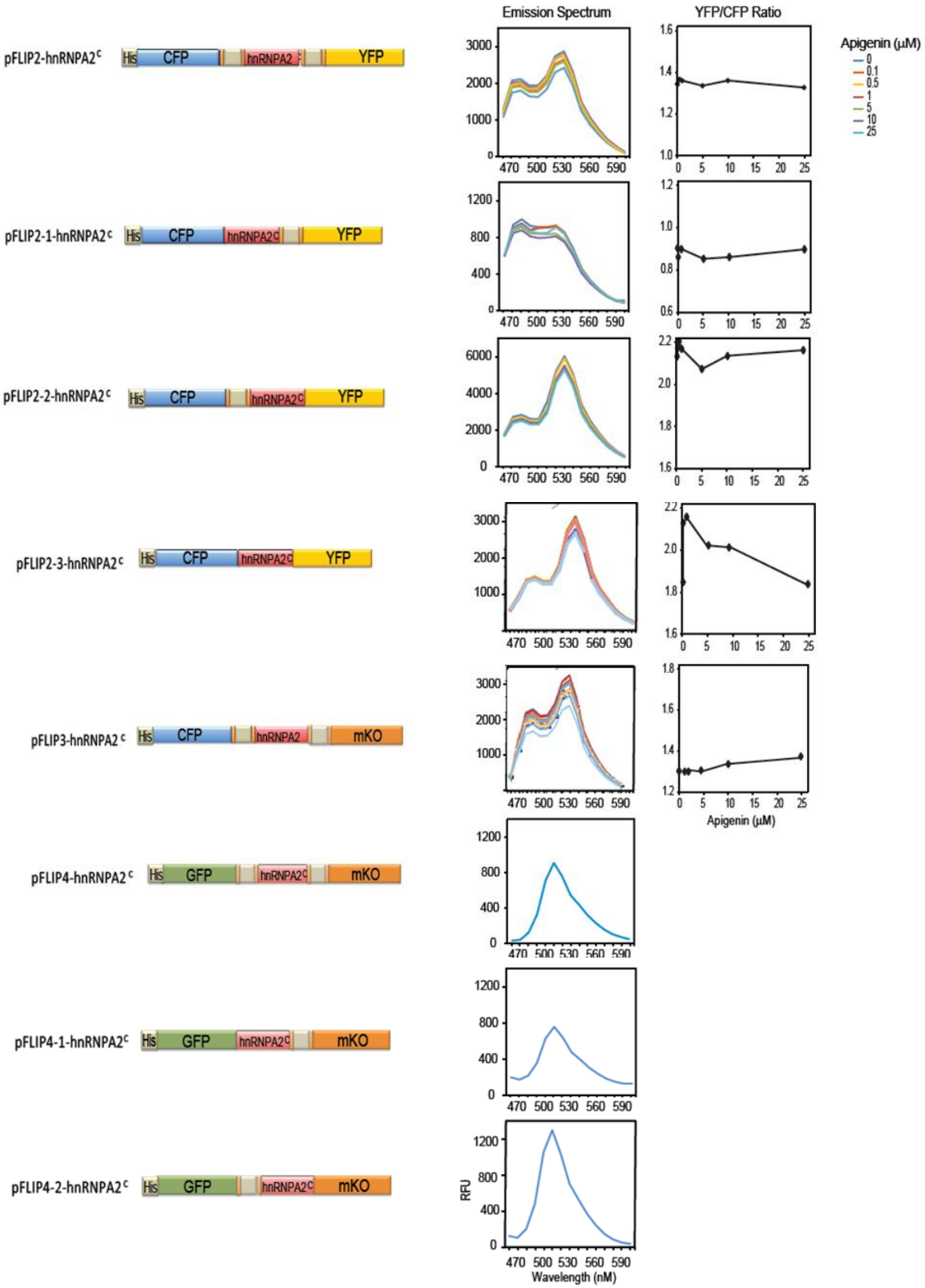

Figure 7. FRET experiments of pFLIP constructs in bacterial lysates. Bacterial lysates were obtained afte bacteria containing the appropriate pFLIP construct shown. Lysates were incubated with increasing co apigenin for 1h and tested for their FRET capabilities by exciting the N-terminal fluorescent protein (ref. Methods) and recording emission over the 460-600 nm spectrum. FRET ratios were calculated for the co showed energy transfer between the fluorescent proteins.

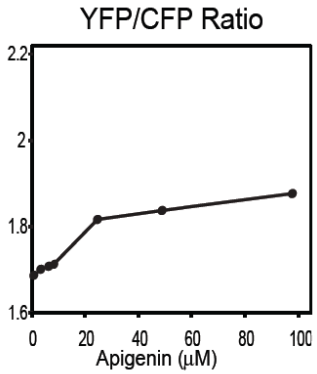

Figure 8. Apigenin binding to FRET nanosensor in bacterial lysates. YFP/CFP ratio of FLIP-2-3-hnRNPA2^{c} incubated with increasing concentrations of apigenin (0, 1, 5, 10, 25, 50 and 100 μM) for 3h at 37^{o}C.

while at the same time preserving the FRET capabilities of the protein, as at later times, FRET was diminished. In order to improve our results, and overcome variability possibly caused by the interaction of the FRET nanosensor with the multiple proteins present in the bacterial lysates, we decided next to purify FLIP-2-3-hnRNPA2^{c}.

Native FLIP-2-3-hnRNPA2^{c} (Figure 9a) protein was purified by Ni^{2+} - NTA affinity column chromatography. Recombinant protein was purified from lysed bacteria using affinity column chromatography for the 6X Histidine tag on the pFLIP-2-3-hnRNPA2^{c} vector (described in Materials and Methods). The protein was eluted using a discontinuous imidazol gradient and run on a SDS-PAGE gel. The gel was stained with coomassie and FLIP-2-3-hnRNPA2^{c} was found eluting at a concentration of 20 and 50 mM imidazole (Figure 9b). These imidazole fractions that contained FLIP-2-3-hnRNPA2^{c} were dialyzed and used for subsequent experiments. The purified FLIP-2-3-hnRNPA2^{c} nanosensor was used to determine the association of hnRNPA2 with apigenin.

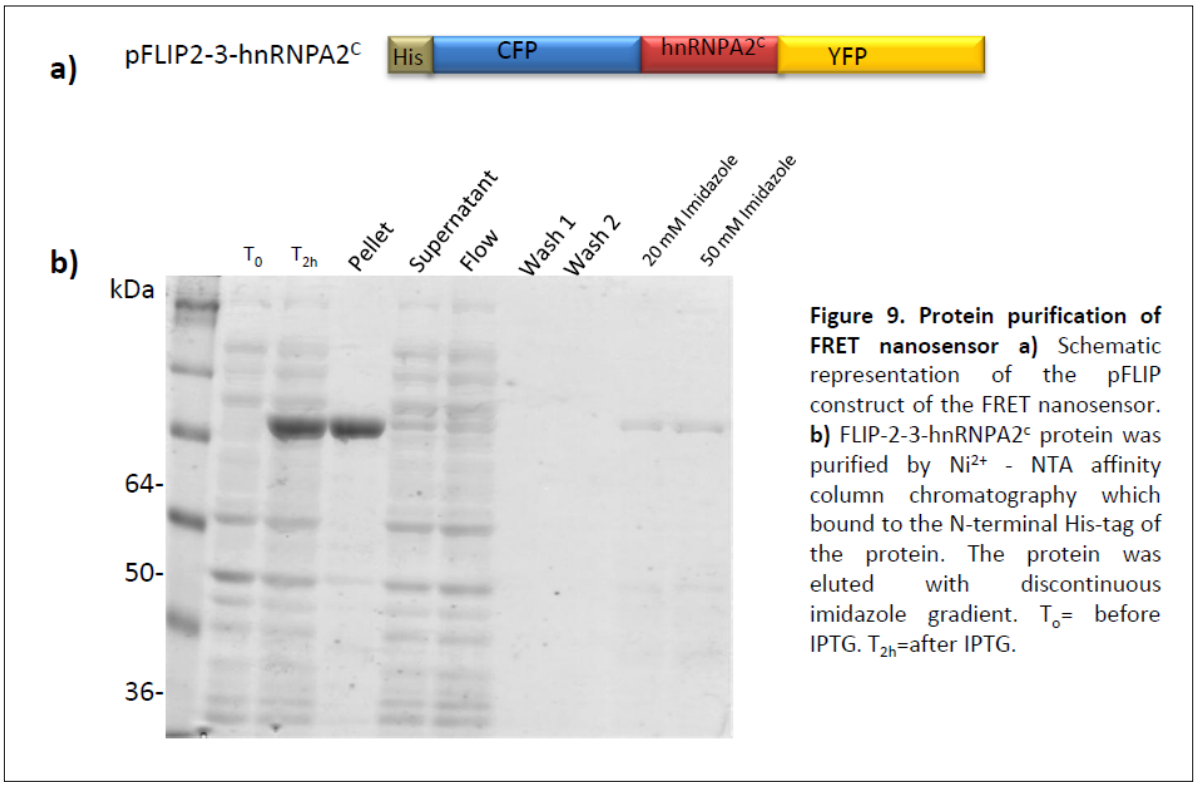

Figure 9. Protein purification of FRET nanosensor a) Schematic representation of the pFLIP construct of the FRET nanosensor. **b)** FLIP-2-3-hnRNPA2^{c} protein was purified by Ni^{2+} - NTA affinity column chromatography which bound to the N-terminal His-tag of the protein. The protein was eluted with discontinuous imidazole gradient. T_o= before IPTG. T_{2h}=after IPTG.

3.3 Multiple Flavonoids Interact with hnRNPA2

To determine the interactions of the purified FLIP-2-3-hnRNPA2^{c}, one micromolar nanosensor was incubated with increasing concentrations of apigenin (0, 1, 5, 10, 25, 50, 100 µM) for 3 h at 37^{o}C, at which time spectrofluorometry was performed and FRET ratios were calculated. The results yielded by the FRET nanosensor incubation with apigenin showed that there was an increase in FRET between the two fluorescent proteins in response to increasing concentrations of apigenin. We conclude therefore that there is an interaction between hnRNPA2 and apigenin (Figure 10a). Further, the data calculated for the YFP/CFP ratios were transformed to saturation curves as described in Materials and Methods. The saturation curves allowed for the calculation of dissociation constants (K_D). For apigenin, the calculated K_D with the hnRNPA2 nanosensor was 22.9 $\pm$ 7.70 µM.

To determine if other structurally similar flavonoids also interacted with hnRNPA2, we incubated indicated flavonoids with the FRET nanosensor. In contrast to apigenin, naringenin (Figure 10c), an apigenin precursor which does not share the physiological benefits of apigenin [27] and differs in structure by a double bond between the two and three carbon positions (Figure 2a), did interact with the FRET nanosensor. Naringenin belongs to the flavonone family of flavonoids, as does eriodictyol (Figure 10c), which did not show binding affinity for the nanosensor and consequently hnRNPA2. Continuing to investigate similar flavonoids to apigenin, we tested luteolin. Luteolin is also classified as a flavone (Table 1), differing from apigenin with an extra alcohol group on the 3' carbon (Figure 2a), which showed binding to hnRNPA2 (K_D = 131 $\pm$ 78.8 µM, Figure 10b). However the addition of a methyl group to the alcohol on the 3' carbon, transforming the molecule into chryseriol, diminishes the interaction (Figure 10b).

The apigenin glucosides, apigein-7-*O*-glucoside and apigenin-6-*C*-glucoside were also tested for their ability to bind hnRNPA2. The 7-*O*-glucoside showed no binding (Figure 10d) while the 6-*C*-glucoside proved to have a more significant interaction to hnRNPA2 (Figure 10d) with a K_D of 60.88 $\pm$ 24.14 µM. This observation highlights the importance of the 7-*O* group in the apigenin interaction with hnRNPA2, as the role of glucose does not seem to be purely steric, as shown by the 6-*C*-glucoside binding. The testing of the glucosides gives insight at to the bio-availability of active apigenin, since the most abundant forms of apigenin are found as glucosides. Interestingly, the flavonols quercetin (K_D = 126 $\pm$ 60.2 µM) and kaempferol (K_D = 27.1 $\pm$ 12.2 µM, Figure 10e), which share similar biological activities as apigenin also showed

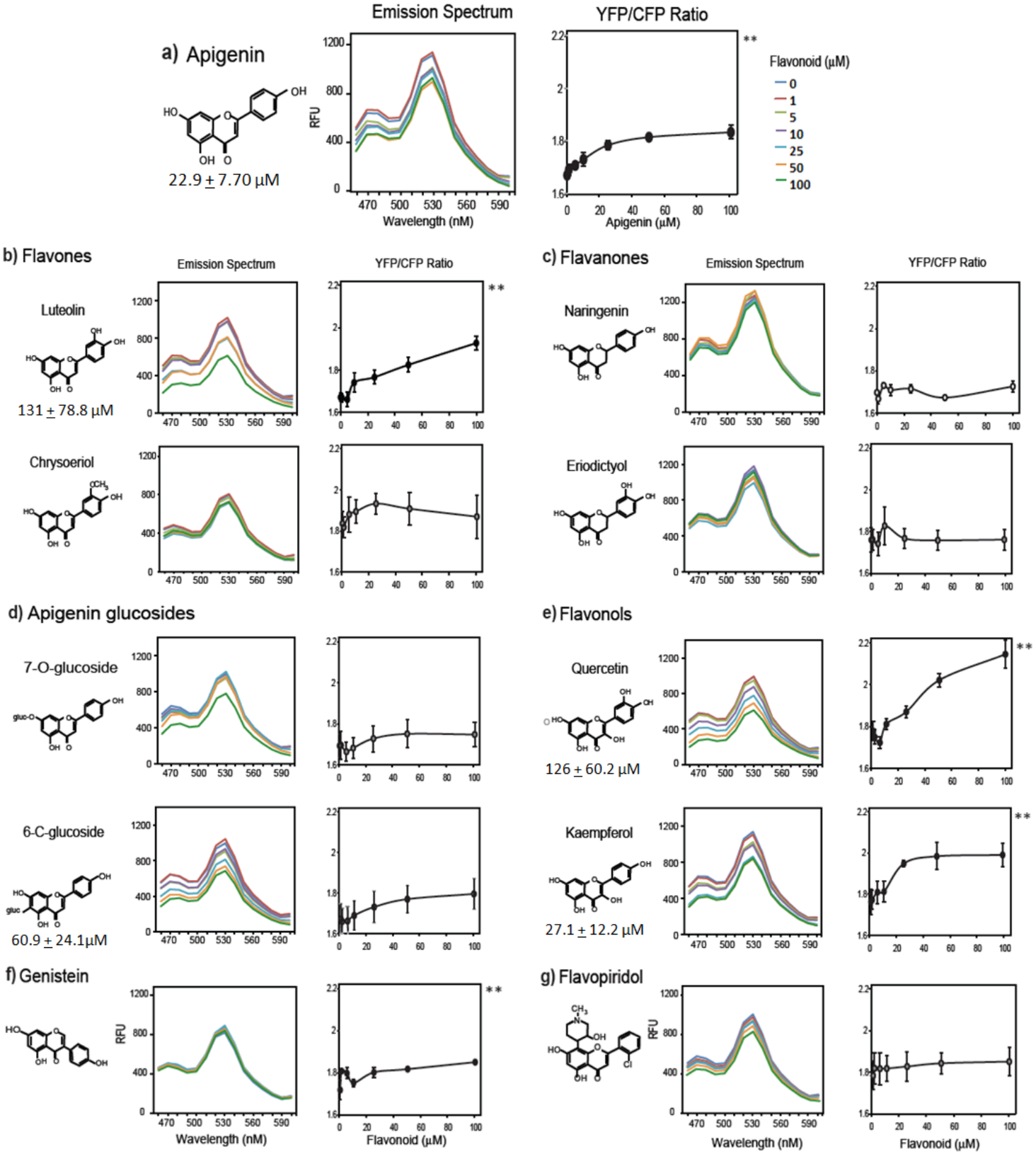

Figure 10. Interactions of FRET-based nanosensor and flavonoids (a-g) The affinity-purified (Refer Materials and Methods) FLIP2-3-hnRNPA2^{C} protein was incubated with increasing concentrations (0, 1, 5, 10, 25, 50 and 100 µM) of the indicated flavonoids for 3 h at 37 °C. Relative fluorescence units (RFU) were determined by spectrofluorometry (l_{ext}: 405 nm; l_{emi}: 460-600 nm) and represented as emission spectra. The calculated YFP/CFP fluorescent ratios (530 nm/480 nm) are also represented over the 0 – 100 µM concentration range for each flavonoid. The molecular structures of the corresponding flavonoids are also shown as are selected K_D values. Data represents the mean ± SEM, n = 3. Statistical significance of the variation of the observed YFP/CFP ratios over the tested flavonoid concentration range was conducted by one-way ANOVA. ** Represents curves with $p < 0.05$

bindig to hnRNPA2. This suggests that they may act in a similar manner as apigenin through hnRNPA2. Alternatively, no binding was detected for the biologically isoflavone genistein (Figure 10f).

Flavonoids such as flavopiridol are currently used in clinical treatment of cancers, and are known to work through their interaction with cyclin dependant kinases [73]. Here we tested the ability of flavopiridol to interact with hnRNPA2. We found that flavopirol (Figure 10g), does not bind to hnRNPA2, suggesting that it works through mechanisms independent of hnRNPA2, as previously known. Together, the results obtained from the flavonoid nanosensor suggest that apigenin and molecularly similar flavonoids bind to hnRNPA2, however slight modifications in structure are capable of disrupting the interaction.

3.4 Apigenin and Invasive Lung Cancer Migration

It has been previously reported that there is an over-expression of hnRNPA2 and its splice variant B1 in all histological subtypes of lung cancers [4], a fact which has lead investigators to explore the role of hnRNPA2 in lung cancer progression and migration. Along with the potential of hnRNPA2 over-expression to be used as an early biomarker for lung cancer, there is the possibility of attacking hnRNPA2 as a therapeutic approach for lung cancer. Microarray data of hnRNPA2/B1 silencing in the adenocarcinoma cell line A549 shows that silencing effects genes involved in cell migration, cellular development and cell death [66]. Other implications of hnRNPA2 involvement in cell migration have exposed the alternative splicing abilities of A2 of genes which affect cell migration, such as T53INP2 [65]. In the study of T53INP2 alternative splicing, hnRNPA2 knockdowns showed both the alternative splicing of the gene, correlated with reduced migration of cells [65]. With these previous results, and the

interaction of apigenin with hnRNPA2, we first investigated the effects of apigenin on hnRNPA2 expression levels and cell migration. Four different non-small lung cancer (NSCLC) cell lines, representing both different stages and histological subtypes, A549 (adenocarcinoma; Stage 1), H2009 (adenocarcinoma; Stage IV), H1703 (Squamous cell carcinoma) and H1299 (Large cell carcinoma) were treated with 0, 1, 10, and 50 μM apigenin for 24 h. mRNA expression levels of hnRNPA2 were evaluated using Real-Time PCR, using 18s ribosomal RNA as a control. We found no significant change in the steady state mRNA levels of hnRNPA2 in cells treated with increasing concentrations of apigenin (Figure 11a). in addition, cell lysates showed no difference in the protein levels of hnRNPA2 in the presence of apigenin (Figure 11b). This suggests that apigenin's interaction with hnRNPA2 does not affect the expression levels of the protein. However, at the 50 μM concentration we found that apigenin decreased hnRNPA2 expression in mouse macrophages and THP-1 monocytic leukemia cells (not shown).

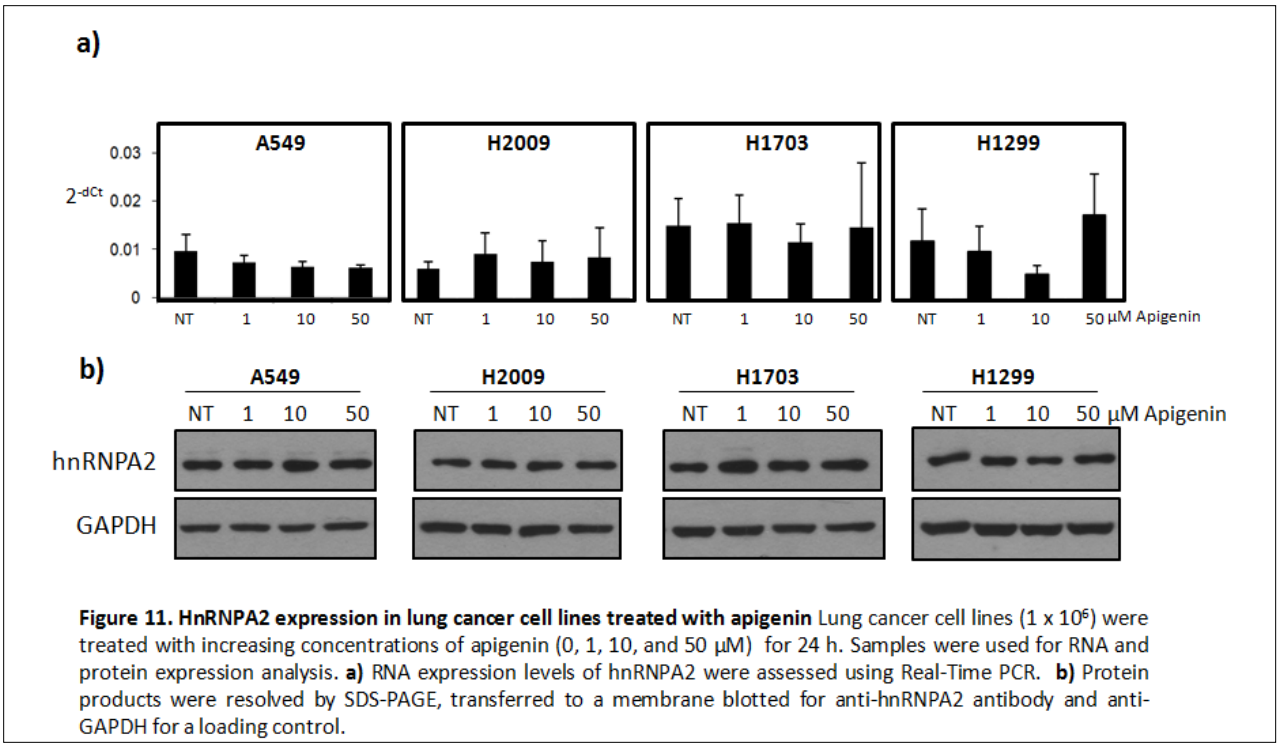

Figure 11. HnRNPA2 expression in lung cancer cell lines treated with apigenin Lung cancer cell lines (1 x 10^6) were treated with increasing concentrations of apigenin (0, 1, 10, and 50 μM) for 24 h. Samples were used for RNA and protein expression analysis. **a)** RNA expression levels of hnRNPA2 were assessed using Real-Time PCR. **b)** Protein products were resolved by SDS-PAGE, transferred to a membrane blotted for anti-hnRNPA2 antibody and anti-GAPDH for a loading control.

We next studied the effect of apigenin in migration, a phenotype associated with hnRNPA2. For this purpose, non-small lung cancer (NSCLC) cell lines were used in scratching assays. The monolayer of cells seeded 16 h before treatment were separated using a pipette tip, creating a space or wound. At this point, apigenin was added at (0, 1, 10, and 50 μM) for 24 h and then cells were photographed at different times to observe the extent of invasive migration. Of the four cell lines, all showed a dose dependant decrease in cell migration when cultured in the presence of apigenin compared to the control (Figure 12). The stage IV adenocarcinoma cell line H2009 had the most aggressive migratory abilities, almost completely closing the wound. However, we found that there is a larger response to apigenin in the later stage IV adenocarcinoma cell line H2009 over the earlier stage A549 with increasing apigenin concentrations. H1703 squamous cell carcinoma cells showed the second most aggressive migration, followed by H1299, large cell carcinoma. All together, apigenin was able to decrease the amount of migration in the lung cancer cell lines. We determined that the more aggressive the cell line, the greater effect apigenin had on migration. We also observed different morphology in all of the lung cancer cells in response to apigenin treatment. The morphology of the cells was of a more compact and less confluent nature, consistent with studies of cell migration in hnRNPA2 knockouts [65]. These results show the potency of apigenin to decrease the invasive migration of lung cancers, with the most significant effect on the aggressive Stage IV adenocarcinoma which reeks havoc on the body through its destructive migratory abilities.

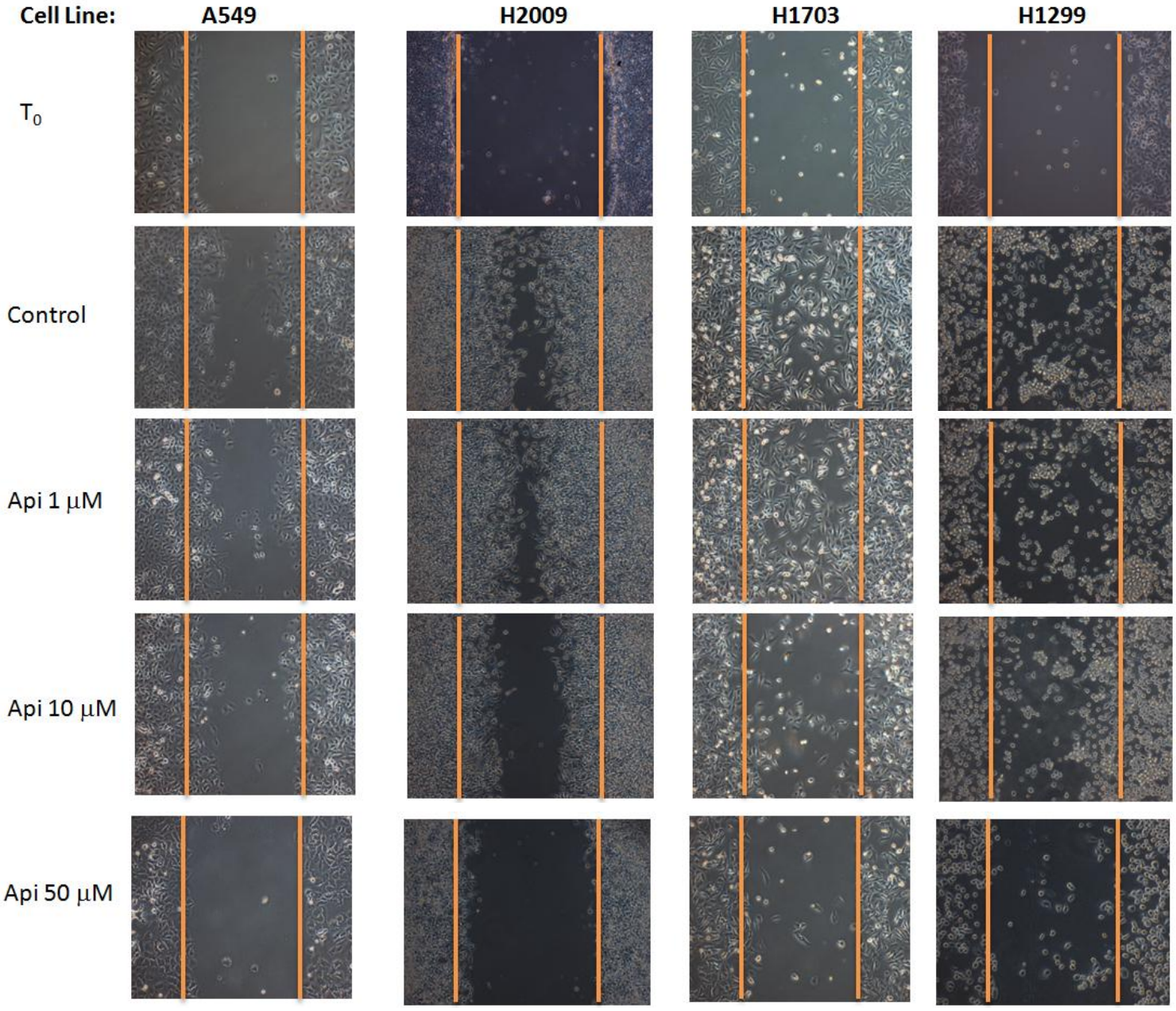

Figure 12. Apigenin and lung cancer migration Lung cancer cell lines representing four different histological subtypes of non-small cell lung cancer were treated with increasing concentrations of apigenin (0, 1, 10, and 50 μM) and monitored for the ability of the cells to migrate after separation of the cells utilizing the "scratch method." Cells were separated and treated with the appropriate concentration of apigenin and incubated for 24 h, at which point the extent of invasive migration was photographed. A549 (adenocarcinoma; Stage I), H2009 (adenocarcinoma; Stage IV), H1703 (Squamous cell carcinoma) and H1299 (Large cell carcinoma).

4. Discussion

The flavonoid apigenin, which is abundantly distributed in a variety of green-leaf plants and vegetables, has many beneficial health properties [10, 11]. These include anti-inflammatory, anti-proliferative and anti-carcinogenic properties [24-26]. The aptitude of apigenin and similar compounds to poses these medically relevant abilities has been long known, however an understanding of the mechanisms by which they act has been lacking. Flavonoids, particularly flavonols and flavones have been shown to interact with extracellular proteins collagen and BSA with dissociation constants (K_D) in the 5 – 100 μM range [74]. In order to address the necessity of knowledge in the mechanisms by which flavonoids work, we utilized a phage-display library with next-generation sequencing to identify, amongst others, the heterogeneous nuclear ribonucleoprotein A2 (hnRNPA2) as a direct target of apigenin. Phage-display is an ideal technique to find cellular targets of small molecules because of the ability to screen a large cohort of proteins in an efficient manner. Phage-display studies have been used to better characterize the cellular interactions of small molecules such the chemotherapeutic paclitaxel [75]. Paclitaxel was known to arrest mitosis and induce apoptosis, however there was no known molecular target by which it acted to induce apoptosis. Through phage-display experiments the anti-apoptotic protein Bcl-2 was identified as a paclitaxol-binding protein [75]. Similarly, apigenin has lacked a cellular target which would shed light onto its mechanism of action. The identified apigenin target, hnRNPA2 is one of approximately 20 major polypeptides in the hnRNP family which are responsible for mRNA metabolism, as well as other actions involving interactions with poly-nucleotides [38]. Notably, hnRNPA2 has been reported to be overexpressed in all histological subtypes of lung cancer as well as a multitude of other carcinomas, making the discovery that it interacts with apigenin even more significant [66]. With

the description of a novel target for the flavonoid apigenin, we investigated if other flavonoids, which include a great diversity of molecules, may function through a similar mechanism. achieve such a goal, we developed a flavonoid nanosensor capable of distinguishing which flavonoids interact with hnRNPA2 as a possible means of exerting their physiological effects. Therefore, we divulged deeper into the interaction of hnRNPA2 with flavonoids to describe novel observations with implications for both cancer and inflammation.

The identified target was validated using pull downs in cellular extracts. In addition, to validate and define the affinity of the interaction between apigenin and hnRNPA2, we constructed a genetically encoded FRET nanosensor. The FRET nanosensor would allow us to both monitor the interaction of apigenin to hnRNP, as well as give us the capability to evaluate a variety of flavonoids and their ability to interact with the protein. In constructing the nanosensor, we cloned human hnRNPA2^{C} (Fig. 3) into the pFLIP2 vector in frame between the regions coding for the N-terminal-CFP and C-terminal-YFP fluorescent proteins. Our studies with the FRET nanosensor validated the hnRNP A2 and apigenin interaction (K_D = 22.9 $\pm$ 7.70 µM) as well as that of flavonoids including luteolin (K_D = 131 $\pm$ 78.8 µM), quercetin (K_D = 126 $\pm$ 60.2 µM) and kaempferol (K_D = 27.1 $\pm$ 12.2 µM). Incubation of the nanosensor with glucosides of apigenin, which are the most abundant natural forms, gave us insight into the bio-aviliblity of apigenin to serve its physiological functions. The addition of a glucose to the apigenin molecule significantly decreased binding of apigein-7-*O*-glucoside and apigenin-6-*C*-glucoside (K_D = 60.88 $\pm$ 24.14 µM). The FRET-nanosensor also provided insight into the structural and functional groups that were most important for apigenin binding to hnRNPA2. This is an attractive feature of the nanosensor which could be exploited to design molecules similar to apigenin that would have a higher affinity for hnRNPA2, thereby, attaining a therapeutic with

comparable potency to that of current chemotherapeutics such as the clinically used flavonoid-based agent flavopiridol, which does not bind to hnRNPA2, but instead works through interactions with cyclin-dependant kinase 9 (Cdk9) to arrest cell division [73]. FRET-based nanosensors are currently used to measure the uptake of vital sugars in multiple organisms [75], technology that can be extended further to measure levels of appropriate flavonoids in solution. This utility could become a tool to be refined for efficient and widespread studies in measuring dietary and supplementary uptake of flavonoids within patients.

In addition, we atempted to follow up on previously published data on hnRNPA2 siRNA experiments, which had showed a decrease in the invasive migration of lung cancer cell lines [65]. We first looked into the effect apigenin-hnRNPA2 interaction on hnRNPA2 expression, as a possible point of hnRNPA2 regulation by apigenin. However, we did not observe a change in hnRNPA2 expression levels at the transcriptional or translational level (Figure 10). We continued with the migration studies to investigate whether the flavonoid-protein interaction would still yield a phenotype observed by the hnRNPA2 knockdown studies. Indeed, we found that the four non-small lung cancer cell lines we studied (A549, H2009, H1703 and H1299) all showed a decrease in migration inversely proportional to apigenin treatment (Figure 11). This suggests to us that the interaction between the apigein and the hnRNPA2, specifically with the Glycine-rich domain (GRD) does not affect the amount of hnRNPA2 in the cell, however, by binding to the GRD and consequently the protein-protein binding domain of A2, apigenin interferes with ability of the protein to dimerize and perform its functions.

In this role, apigenin is serving as a regulator of hnRNPA2 and its downstream effects. The apigenin bound, less physiologically active effects of hnRNPA2 may include the differential alternative splicing reported for the pyruvate kinase (PK) and TP53INP2 genes involved in

cancer growth and migration respectively, to their non-carcinogenic isoforms (Figure 13. Model of apigenin molecular mechanisms). Another possibility by which apigenin bound to hnRNPA2 could be impacting cell migration is through its anti-inflammatory effects. In the inflammatory pathway, when ligands such as lipopolysaccharide (LPS) bind to toll-like receptors (TLR), it triggers a signaling cascade which culminates in the phosphorylation of the IKK complex by casein kinase 2 (CK2) and subsequent release of the transcription factor NF-κB (Figure 13). NF-κB upregulates chemokine receptor CXCR4, which when bound by its ligand stromal cell-derived factor (SDF-1) plays a major role in cellular movement [76]. The CXCR4/SDF-1 axis is involved in embryogenesis and organogenesis and plays an important role in directing hematopoetic/lymphopoeitic stem cells to inflammation sites [77-79]. Interestingly, higher CXCR4 increases metastasis of lung cancer where reduced expression and localization of CXCR4 in the nucleus correlates with a better outcome [80]. Pan *et al*, proposed that the observed CXCR4 mediated migration of cells may be related to CXCR4-mediated nuclear export of hnRNPA2/B1 [81]. Therefore, triggering of inflammation leads to the activation of NFκB, causes the upregulation of CXCR4, increases the extranuclear concentration of hnRNPA2/B1 and causes the migration of cells and other effects of hnRNPA2/B1 overexpression. Apigenin interferes with this pathway by blocking the effects of the hnRNPA2/B1 overexpression, and down-modulating its pro-carcinogenic effects.

Further evidence for this model comes from the interaction of hnRNPA2 and CK2. CK2 phosphorylation of hnRNPA2 represents a post-translational modification of hnRNPA2 with yet unknown consequences. It has also been shown that hnRNPA2 associates with the catalytic subunit of CK2 [82]. As previously stated, CK2 is responsible for the phosphorylation of the IKK complex to release NF-κB transcription factor, and may be another point where apigenin

binding to hnRNPA2 can be modulating the protein's interaction with CK2. This step in the pathway is also directly impacted by apigenin's inhibition of CK2. However of the multitude of interactions described need to be further investigated to assess their outcomes on cell migration, proliferation and inflammation. It would seem that the overexpression and differential localization of hnRNPA2 is the consequence of multiple pathways, and extranuclear localization of hnRNPA2 is associated with a poor prognosis. Interestingly, internal data suggests that apigenin is also localized in the cytosol and not the nucleus. HnRNPA2 is heavily involved in cell migration of both normal and cancer cells. However under cancerous conditions, hnRNPA2 expression does not return to normal after proper migration [83]. We have shown that apigenin is able to bind hnRNPA2 and that apigenin treatment inhibits migration of cells. We therefore conclude that apigenin binding to hnRNPA2 inhibits the proteins pro-migratory effects.

For our future directions, we will delve deeper into the physiological relevance of the apigenin-hnRNPA2 interaction. We will do this firstly by introducing the FRET-based nanosensor into mammalian cells and monitoring apigenin uptake and interaction and binding to the nanosensor *in vivo* to provide further evidence of the stable protein-ligand interaction. Also, we need to look into the alternative splicing by hnRNPA2 in response to apigenin treatment, to see if we can replicate the same results as presented by the studies with pyruvate kinase (PK) and TP53INP2 of hnRNPA2 knockdowns. This will give us more definitive proof of the observed anti-migratory and anti-proliferative phenotypes of apigenin on lung cancer cell lines. Finally, hnRNPA2 and its functions are not able to explain all of the physiological roles of apigenin. Thus, we must also investigate the other direct targets of apigenin identified by our phage-display studies, continuing to validate more targets, in order to provide a holistic representation of apigenin's effects.

Figure 13. Model of apigenin molecular mechanisms

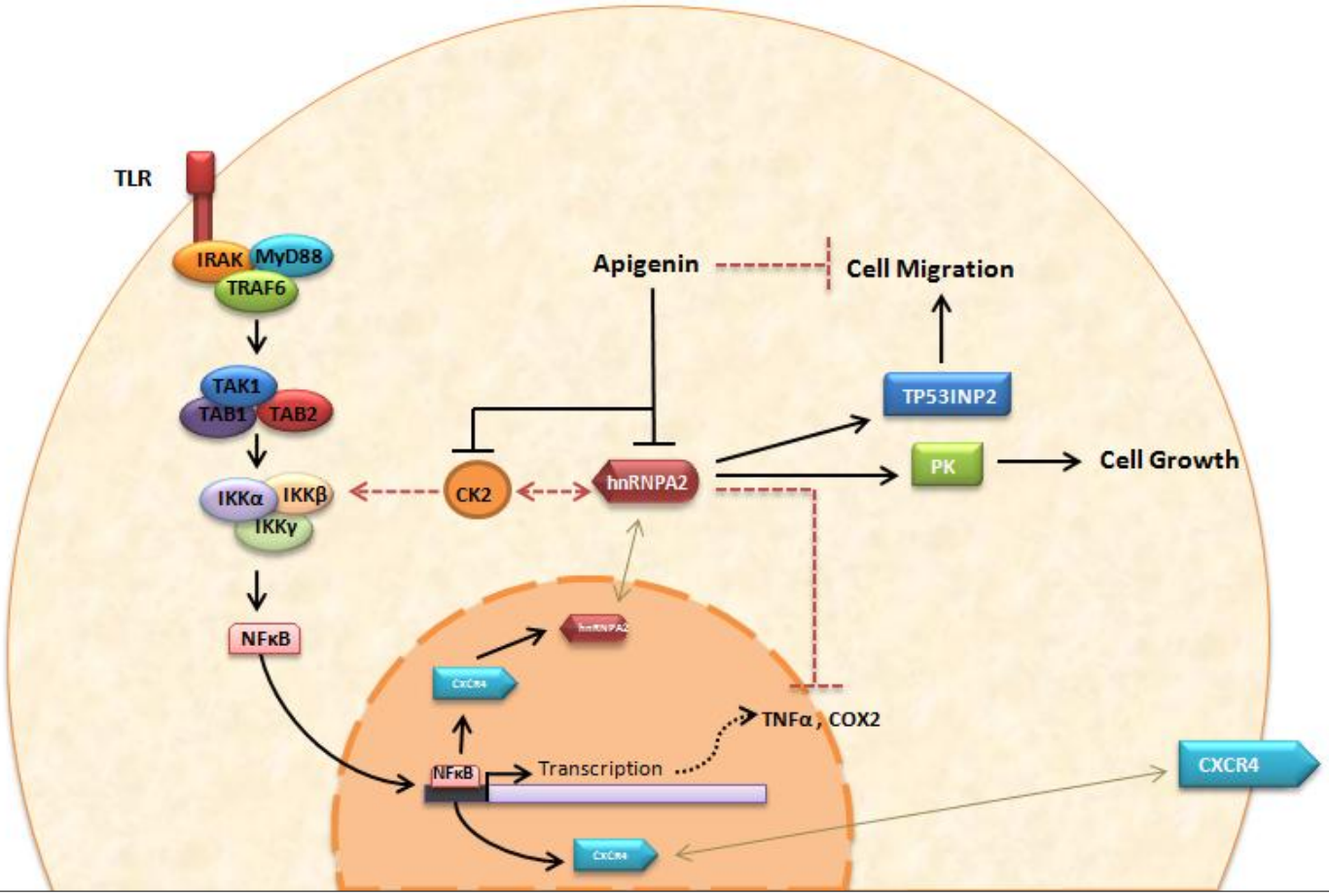

Acknowledgements

Thanks to Dr. Andrea Doseff for her mentoring, opportunity to perform research, and critical reading of this thesis. Thanks also to Daniel Arango for his contribution to this work and the Doseff lab members for their aid and support. Thank you to Dr Wolf Frommer for his generous gift of the pFLIP vectors. This work was supported by National Institutes of Health (NIH)/National Heart, Lung, and Blood Institute (NHLBI) R01HL075040-01 to A.I.D.

References

1. Wolrd Health Organization: Cancer, 2011.
2. Hahn WC, Weinberf RA. Modeling the molecular circuitry of cancer. Nat Rev Cancer 2002; 2:331-341.
3. Austoker J. Cancer prevention in primary care. Current trends and some prospects for the future. BMJ 1994;309:517-520.
4. Katsimpoula S, Patrinou-Georgoula M, Makrilia N, Dimakou K, Guialis A, Orfanidou D, Syrigos KN. Overexpression of hnRNPA2/B1 in bronchoscopic speciments: a potential early detection marker in lung cancer. Anti-Cancer Res 2009; 29: 1373-1382.
5. PubMed Health: Lung Cancer. http://www.ncbi.nlm.nih.gov/pubmedhealth/PMH0004529/
6. Zang Z, Ma J, Li N, Sun N, Wang C. Expression of nuclear factor-kappaB and its clinical significance in non-small cell lung cancer. AnnThorac Surg 2006; 82: 243-8.
7. Scglioni PP, Yung TM, Choi SC, Baldini C, Konstantinidou G, Pandolfi P. CK@ mediates phosphorylation and ubiquitin-mediated degredatino of the PML tumor suppressor. Mol Cell Biochem 2008; 316: 149-54.
8. Stahl S, Branca R, Efazat G, Ruzzene M, Zhivotovsky B, Lewensohn R, Viktorsson K, Lehtjo J. Phosphoproteomic profiling of NSCLC cells reveals that ephrin B3 regulates pro-survival signaling through Akt1-mediated phosphorylation of the EphA2 receptor. J Proteome Res 2011.
9. Alberg AJ, Ford JG, Samet JM: Epidemiology of lung cancer: ACCP evidence-based clinical practice guidelines (2nd edition). Chest 2007; 132:29S-55S.
10. Shukla S, Gupta S. Apigenin: a promising molecule for cancer prevention. Pharm Res 2010; 27: 962-78.
11. Kris-Etherton PM, Hecker KD, Bonanome A, Coval SM, Binkoski AE, Etherton TD. Bioactive Compounds in Foods: Their Role in the Prevention of Xardiovascular Disease and Cancer. Am J Med 2002;113:71S-88S.
12. Yildz L, Baskan KS, Tutem E, Apak R. Combined HPLC-CUPRAC 9cupric ion reducing antioxidant papacity) assay of parsley, celery leaves and nettle. Talanta 2008; 77(1):302-313.
13. Manach C, Scalbert A, Morand C, Remesy C and Jimenez L. Polypehnols: food sources and bioavailability. Am J Clin Nutr 2004; 70: 727-747.
14. Yang CS, Landau JM, Huang MT and Newmark HL. Inhibition of carcniogenesis by dietary polypehnolic compounds. Annu Rev Nutr 2001; 21: 831-406.
15. Williams RJ, Spencer JP, Rice-Evans C. Flavonoids: antioxidants or signaling molecules. Free Radic Biol Med 2004; 36: 838-49.
16. Tunon MJ, Garcia-Mediavilla MV, Sanchez-Campos S, Gonzalez-Gallego J. Potential of flavonoids as anti inflammatory agents: modulation of pro-inflammatory gene expression and signal transduction pathways. Curr Drug Metab 2009; 10: 256-71.
17. Gray N, Detivaud L, Doerig C, Meijer L. ATP-site directed inhibitors of cyclin-dependent kinases. Curr Med Chem 1999; 6: 859-75.
18. Virk-Baker MK, Nagy TR, Barnes S. Role of phytoestrogens in cancer therapy. Planta Med 2010; 76: 1132-42.
19. Hertog MG, Feskens EJ, Hooman PC, Katan MB, Kromhout D. Dietary flavonoids and cancer risk in the Zutphen Elderly Study. Nutr Cancer 1994;22:175-184.

20. Hoensch H, Groh B, Edler L, Kirch W. Prospective cohort comparison of flavonoid treatment in patients with resected colorectal cancer to prevent recurrence. World J Gastroenterol 2008;14:2187-2193.
21. Cheung ZH, Leung MC, Yip HK, Wu W, Siu FK, So KF. A neuroprotective herbal mixture inhibits caspase-3-independent apoptosis in retinal ganglion cells. Cell Mol Neurobiol 2008;28:137-155.
22. McKay DL, Blumberg JB. A review of the bioactivity and potential health benefits of chamomile tea (Matricaria recutita L.). Phytother Res 2006;20:519-530.
23. Svehlikova V, Bennett RN, Mellon FA, Needs PW, Piacente S, Kroon PA, Bao Y. Isolation, Identification and stability of acylated derivatives of apigenin 7-O-glucoside form chamomile. Phytochemistry 2004: 65: 2323-2332.
24. Gupta S, Afaq F, Mukhtar H. Selective growth-inhibitory, cell-cycle deregulatory and apoptotic response of apigenin in normal versus human prostate carcinoma cells. Biochem Biophus Res Commun 2001; 287:914-920.
25. Middleton E JR, Kandaswami C, Theoharides TC. The effects of plant flavonoids on mammalian cells: implications for inflammation , heart disease, and cancer. Pharmacol Rev 200;52:673-751.
26. Patel D, Shukala S and Gupta S. Apigenin and cancer chemprevention: Prgress, potential and promise. Int J of Onco 2006; 30; 233-245.
27. Vargo MA, Voss OH, Poustka F, Cardounel AJ, Grotewold E, Doseff AI. Apigenin-induced-apoptosis is mediated by the activation of PKCdelta and caspases in leukemia cells. Bioch Pharmcol 2006; 72: 681-692.
28. Farah M, Parhar K, Moussavi M, Eivemark S, Salh B. 5,6dichlororibifuranosylbenzimidazole (DRB) and apigenin induced sensitization of colon cells to TNFalpha mediated apoptosis. Am J Physiol Gastrointest 2003.
29. Wei H, Tye L, Bresnick E, Birt DF. Inhibitory effect of apigenin, a plant flavonoid, on epidermal ornithine decarvoxylase and skin tumor promotion in mice. Cancer Res 1990;50:499-502.
30. Menichincheri M, Ballinari D, Bargiotti A, Bonomini L, Ceccarelli W, C'alessio R, Fretta A, Moll J, Polucci P, Soncini C, Tibolla M, Trosset JY, Vanotti E. Catecholic flavonoids acting as telomerase inhibitors. J Med Chem 2004:47:6466-6475.
31. Brusselmans K, Vrolix R, Verhoeven G, Swinnen JV. Induction of cancer cell apoptosis by flavonoids is associated with their avility to inhibit fatty acid synthase activity. J Biol Chem 2005;280:5636-5645.
32. MH. Flavonoids inhibit VEGF/bFGF-induced angiogenesis in vitro by inhibiting the matrix degrading proteases. J Cell Biochem 2003;89:529-538.
33. Reiners JJ Jr, Clift R, Mathieu P. Suppression of cell cycle progression by flavonoids: dependence on the aryl hydrocarbon receptor. Carcinogenesis 1999;279:4479-4489.
34. Fahy RJ, Doseff AI, Wewers MD. Spontaneous human monocyte apoptosis utilizes a caspase-3-dependent pathway that is blocked by endotoxin and is independent of caspase-1. J of Immunonolgy 1999; 15:1755-62.
35. Goyal A, Wang Y, Graham MM, Doseff AI, Bhatt NY, Marsh CB. Monocyte survival factors induce Akt activation and suppress caspase-3. Am J Respir Cell Mol Biol 2002; 26:224-230.
36. Aulls JE, Murray PJ. Tumor macrophages protective and pathogenic roles in cancer development. Curr Top Dev Biol 2011; 94: 309-28.

37. Nicholas C, Batra S, Vargo MA, Voss OH, Gavrilin MA, Wewers MD, Guttridge DC, Grotewold E, Doseff AI. 2007; 179: 7121-7.
38. Yaown He and Ross Smith. Nuclear functions of heterogeneous nuclear ribonucleoproteins A/B. Cell and Mol Life Sci 2009.
39. Burd CG, Swanson MS, Gorlach M, Dreyfuss G. Primary structure of the heterogeneous nuclear ribonucleoprotein A2. Proc Natl Acad Sci 1999; 86:9788-9792.
40. Nichols RC, Wang XW, Tang J, Hamilton BJ, High FA, Herschman, Rigby WF. The RGG domain in hnRNPA2 affects subcellular localization. Exp. Cell Res 2000; 256: 522-532.
41. Beyer AL, Christensen ME, Walker BW, LeStourgeon WM. Identification an characterization of the packaging proteins of core 40s hnRNP particles. Cell 1977; 127-138.
42. Donev R, Horton R, Beck S, Doneva R, Bowen WR, Scheer D. Recruitment of heterogeneous nuclear ribonucleoprotein A1 in vivo to the LMP/TAP region of the major histocompatibility complex. J Biol Chem 2003; 278: 5214-5226.
43. Munro TP, Magee RJ, Kidd GJ, Carson JH, Barbarese E, Smith LM, Smith R. Mutational analysis of a heterogeneous nuclear ribonucleoprotein A2 response element for RNA trafficking. J Biol Chem 1999; 274: 34389-3495.
44. Ainger K, Avossa D, Diana AS, Barry C, Barbarese E, Carson JH. Transport and localization elements in myelin basic protein mRNA. J Cell Biol 1997; 138: 1077-1087.
45. Hoek KS, Kidd GJ, Smith R. hnRNPA2 selectively binds the cytoplasmic transport sequence of melin basic protein mRNA. Biochemistry 1998; 37: 7021-7029.
46. Moran-Jones K, Wayman L, Kennedy DD, Reddel R, Sara S, Snee MJ, Smith R. hnRNPA2, a potential ssDNA/RNA molecular adapter at the telomere. Nucleic Acids Res 2005; 33: 486-496.
47. Gao Y, Tatavarty V, Korza G, Levin MK, Carson JH.Multiplexed dendritic targeting of alpha calcium calmodulin-dependent protein kinase II, neurogranin, and activity-regulated cytoskeleton-associated protein RNAs by the A2 pathway. Mol Biol Cell 2008; 19:2311-27.
48. Mouland AJ, Xu H, Cui H, Krueger W, Munro TP, Prasol M, Mercier J, Rekosh D, Smith R, Barbarese E, Cohen EA, Carson JH. RNA trafficking signals in human immunodeficiency virus type 1. Mol Cell Biol 2001; 21: 2133-2143.
49. Kajita Y, Nakayama J, Aizawa M, Ishikawa F. The UUAG-specific RNA binding protein, heterogeneous nuclear ribonucleoprotein D0. Common modulator structure and binding properties of the 2xRBD-Gly family. J Biol Chem 1995; 270: 22167-22175.
50. Shan J, Moran-Jones K, Munro TP, Kidd GJ, Winzor DJ, Hoek KS, Smith, R. Binding of an RNA trafficking response element to heterogeneous nuclear ribonucleoproteins A2 and A2. J Biol Chem 2000; 275: 38286-38295.
51. Vera J, Jaumot M, Estanyol JM, Burn S, Agell N, Bachs O. Heterogeneous nuclear ribonucleoprotein A2 is a SET-binding protein and a PP2A inhibitor. Oncogene 2006; 25: 260-270.
52. Eddy J, Maizels N. Conserved elements with poetential to form polymorphic G-quadruplex structures in the first intron of human genes. Nucleic Acids 2008; 36: 1321-1333.
53. Iwanaga K, Sueoka N, Sato A, Hayashi S, Sueoka E. Heterogeneous nuclear ribonucleoprotein B1 protein impairs DNA repair mediated through the inhibition of

DNA-dependent protein kinase activity. Biochem Biophys Res Commun 2005; 333: 888-895.
54. McKay SJ, Kooke H. hnRNP A2/B1 binds specifically to single stranded vertebrate telomeric repeat TTAGGGn. Nucleic Acids Res 1992; 20: 6461-6464.
55. LaBranche H, Bupuis S, Ben-David Y, Bani MR, Wellinger RJ, Chabot B. Telomere elongation by hnRNP A1 and a derivative that interacts with telomeric repeats and telomerase. Nat Genet 1998; 19: 199-200.
56. Takimoto M, Tomonaga T, Matunis M, Avigan M, Krutzsch H, Dreyfuss G, Levens D. Specific binding of heterogeneous ribonucleoprotein proticle protein K to the human c-myc promoter, in vitor. J Biol Chem 1993; 263: 18249-18258.
57. Campillos M, Lamas JR, Garcia MA, Bullido MJ, Valdivieso F, Vazquez J. Specific interaction of heterogeneous nuclear ribonucleoprotein A1 with the -219T allelic form modulates APOE promoter activity. Nucleic Acids Res 2003; 31: 3063-3070.
58. Thakur S, Nakamura T, Calin G, Fusso A, Tamburrino J, Shimizu M, Baldassarre G, Battista S, Fusco A, Wassell RP, Dubois G, Alder H, Croce CM. Regulation of BRCA1 transcription by specific single-stranded DNA binding factors. Mol Cell Biol 2003; 23, 3774-3787.
59. Zhao S, Korzan WJ, Chen CC, Fernald RD. Heterogeneous nuclear ribonucleoprotein A/B and G inhibits the transcription of gonatotropin-releasing-hormone. Mol Cell Neurosci 2008; 37: 6984.
60. Rosonina E, Ip JY, Calaroco JA, Bakowski MA, Emili A, McCracken S, Tucker P, Ingles CJ, Blencowe BJ. Role for PSF in mediating transcriptional activator dependent stimulation of pre-mRNA Processing in vivo. Mol Cell Biol 2005; 25: 6734-6746.
61. Kastan MB, Canman CE, Leonard CJ. P53, cell clycle control and apoptosis: implications for cancer. Cancer Metastasis Rev 1995; 14: 3-15.
62. Venables JP, Hoh CS, Froehlich U, et al. Multiple and specific mRNA processing targets for the major human hnRNP proteins. Mol Cell Biol 2008; 28;6033-43.
63. Zhou Z, Licklider LJ, Gygi SP, Reed R. Comprehensive proteomic analysis of the human spliceosome. Nature 2002; 419: 182-185.
64. Charles J, Mo C, Marcela A, Peter C and James M. HnRNP proteins controlled by c-Myc deregulate pyruvate kinase mRNA splicing in cancer. Nature 2010; 436, 364-368.
65. Moran-Jones K, Grindlay J, Jones M, Smith R, Norman JC. hnRNP A2 regulates alternative mRNA splicing of TP53INP2 to control invasive cell migration. Cancer Res 2009; 69: 9219-27.
66. Tauler J, Zudaire E, Liu H, Shih J, Mulshine JL. hnRNP A2/B1 modulates epithelial-mesenchymal transition in lung cancer cell lines. Cancer Res 2010; 15:7137-47.
67. Zhou J, Allred DC, Avis I, et al. Differential expression of the early lung cancer detection marker, heterogeneous nuclear ribonucleoprotein-A2/B1 in nrmal breast and neoplastic cancer. Breast Cancer Res Treat 2001;66:217-24.
68. Lee CH, Lum JH, Cherng BP. Identification of the heterogeneous nuclear ribonucleprotein A2/B1 as the antigen for the gastrointestinal cancer specific monoclonal antibody MG7. Proteomics 2005;5:1160-6.
69. Maggipinto M, Rabiner C, Kidd GJ, Hawkins AJ, Smith R, Barbarese E. Incerase expression of the MBP mRNA binding protein HnRNP A2 dring oligodendrocyte differentiation. J Neruosci Res 2004: 75:614-23.

70. Cheng CY, Kuo CT, Lin CC, Hsieh HL, Yang CM. IL-1beta induces expression of matrix metalloproteinase-9 and cell migration via a c-Src-dependent, growth factor receptor transactivation in A549 cells. Br J Pharmacol 2010 160:1595-610.
71. Lager I, Looger L, Hilpert M, Lalonde S, Frommer WB. Conversion of a putative agrobacterium sugar-binding protein into a FRET sensor with high selectivity for sucrose. J Biol Chem 2006; 281: 30875-83.
72. Fehr M , Lalonde S, Ehrhardt DW, Frommer WB. Live imaging of glucose homeostasis in nuclei of COS-7 cells. J Fluoresc 2004; 14: 603-9.
73. Vladimir K, Stjepan U. Cyclin-Dependent Kinase Inhibitors as Anticancer Drugs. pp.291-302 (12) Current Drug Targets Volume 11 Issue 3 ISSN: 1389-4501
74. Dangels O, Dufour C. Flavonoids: Chemistry, Biochemistry and Applications (eds. Anderson OM, Markham KR) 2006: 443-469.
75. Rodi DJ, Janes RW, Sanganee HJ, Holton RA, Wallace BA, Makowski L. Screening of a library of phage-displayed peptides identifies human Bcl-2 as a Taxol-binding protein. J Mol Biol 1999; 285: 197-203.
76. Ratajcak MZ, Majka M, Drukala J, Pietrzkowski Z, Peiper S, Janowska-Wieczorek A. Expression of functional CXCR4 by muscle satellite cells and secretion of SDF-1 by muscle-derived fibroblasts is associated with the presence of both muscle progenitors in bone marrow and hematopoietic stem/progenitor cells in muscles. Stem Cells 2003, 21:363-371.
77. Stumm RK, Zhou C, Ara T, Lazarini F, Dubois-Dacq M, Nagasawa T, Hoolt V, Schulz S: CXCR4 regulates interneuron migration in the developing neocortex. J Neurosci 2003, 23:5123-5130
78. Lazarini F, Tham TN, Casanova P, Arenzana-Seisdedos F, Dubois-Dalcq M: Role of the alpha-chemokine stromal cell-derived factor (SDF-1) in the developing and mature central nervous system. GLIA 2003, 42:139-148.
79. Ratajczak MZ, Kucia M, Reca R, Majka M, Janowska-Wieczorek A, Ratajczak J: Stem cell plasticity revisited: CXCR4-positive cells expressing mRNA for early muscle, liver and neural cells 'hide out' in the bone marrow. Leukemia 2004, 18:29-40.
80. Spano JP, Andre F, Morat L, Savatier L, Besse B, Combadiere C, Deterre P, Martin A, Azorin J, Valeyre D er al.:Chemokine receptor CXCR4 is associated with the metastatic potential of human non-small cell lung cancer: pattern of expression and correlation with outcome. Ann Oncol 2004, 15:613-617.
81. Yoo Y, Wu X, Egile C, Li R, Guan JL: Interaction of N-WASP with hnRNPK and its role in filopodia formation and cell spreading. J Biol Chem 2006, 281:15352-15360.
82. Pancetti F, Bosser R, Krehan A, Pyerin W, Itarte E, Bachs O. Heterogeneous nuclear ribonucleoprotein A2 interacts with protein kinase CK2.
83. Peebles KA, Dwyer-Nield LD, Malkinson AM. Altered expression of splicing factor, heterogenewous nuclear ribonucleoprotein A2/B1, in mouse lung neoplasia. Mol Carcinog 2007;46:887-900.